THE ASTROPHYSICAL JOURNAL, 241:279–299, 1980 October 1

OUTER ATMOSPHERES OF COOL STARS. V. *IUE* OBSERVATIONS OF CAPELLA: THE ROTATION-ACTIVITY CONNECTION

T. R. AYRES[1] AND J. L. LINSKY[1,2]
Joint Institute for Laboratory Astrophysics, University of Colorado and National Bureau of Standards
Received 1979 August 6; accepted 1980 April 8

ABSTRACT

We present and analyze ultraviolet spectra of Capella (G6 III + F9 III) obtained with the *International Ultraviolet Explorer*. High-dispersion spectra in the 1150–2000 Å region taken at orbital velocity crossing show no evidence for the increasing blueshifts with increasing temperature of formation previously inferred from *Copernicus* observations. We conclude that there is no discernible stellar wind from either component of the system. High-resolution emission-line profiles taken near the elongation at phase 78 days suggest that virtually all of the emission in transition-region (TR) lines (2×10^4 K $\leq T \leq 2 \times 10^5$ K) and most of the emission in chromospheric lines ($T \lesssim 10^4$ K) come from the late-F secondary of the system. This result is contrary to the assumption made in most previous studies that the slightly more massive Capella primary is the dominant ultraviolet emitter. We propose that the origin of the extraordinarily different activity levels on these otherwise very similar stars can be traced to the one property that is obviously different, namely, rotation: the Capella primary is a normal, sharp-lined, slow rotating giant, whereas the secondary has broader lines and is a rapid rotator for a late-type giant ($V \sin i \lesssim 30$ km s^{-1}). Such a chromospheric rotation-activity connection has been demonstrated previously in the Ca II emission cores, and is very likely a consequence of enhanced surface magnetic fields produced by increased dynamo action in rapidly rotating, convective stars. We extend the rotation-activity connection to stellar transition regions and suggest, on the basis of published soft X-ray observations of a limited sample of stars, that it is valid for coronae as well.

Subject headings: stars: atmospheres — stars: chromospheres — stars: individual — stars: late-type — stars: winds — ultraviolet: spectra

I. INTRODUCTION

Important clues to the origins of chromosphere-corona phenomena in cool stars can be uncovered by comparing the Sun with other very different stars. Capella[3] provides such a perspective. Capella consists of a pair of young, but evolved, giant stars, each more massive and more luminous than the Sun, coexisting in a close orbit ($\sim$1 AU), whereas the Sun is a middle-aged, low-mass, single, main-sequence dwarf. Previous work has already revealed significant differences between Capella and the Sun. For example, Dupree (1975) proposed that the Capella primary has a massive—and decidedly nonsolar—stellar wind ($\sim 10^{-8}\ \mathfrak{M}_\odot$ yr^{-1}), based on radial velocity studies of the O VI λ1032 resonance line. Furthermore, ultraviolet and soft X-ray measurements indicated that Capella's outer atmosphere is significantly more active than that of the average Sun (Haisch and Linsky 1976).

Capella was the first cool star observed by the *International Ultraviolet Explorer* (Boggess *et al.* 1978). Short-wavelength echelle mode spectra confirmed the *Copernicus* results of Dupree (1975, 1976) that high-temperature emission lines ($T \sim 10^5$ K) are very broad (FWHM $\gtrsim$ 100 km s^{-1}) and that line surface fluxes (ergs cm^{-2} s^{-1} at the star) are systematically larger than quiet-Sun fluxes by a factor of about 20 if the emission is attributed solely to the Capella primary (Linsky *et al.*1978). The initial *IUE* spectra reinforced the notion that Capella is quantitatively different from solar-type quiet-chromosphere dwarfs, such as α Centauri A and B (G2 V + K1 V; see Ayres and Linsky 1980, hereafter Paper III) and the Sun itself. Subsequently, we obtained additional high-dispersion spectra of Capella at several orbital phases with *IUE*. Our intent was to determine the relative flux contribution of the primary (Aa) and secondary (Ab) to the composite EUV emission spectrum. We also obtained a series of low-dispersion exposures, through both the

[1] Guest observer with the *International Ultraviolet Explorer* satellite.

[2] Staff member, Quantum Physics Division, National Bureau of standards.

[3] Capella (α Aurigae A) is a 104 day spectroscopic binary consisting of a G6 III primary (Capella Aa) and an F9 III secondary (Capella Ab). The α Aurigae system also contains additional, but widely separated and faint, components which are not considered here.

large (10″ × 20″) and small (3″ diameter) apertures, to provide accurate absolute fluxes for the prominent emission features, and to identify the many weak features that are too faint to be detected in the echelle mode spectra.

The preliminary analysis of our data produced two unexpected results. First, we found no evidence for large systematic mass flows at temperatures near 10^5 K compared with cooler layers ($T \sim 6 \times 10^3$–2×10^4 K), contrary to the *Copernicus* results of Dupree (1975, 1976). Second, and most surprising, we found that virtually all of the flux in the high-temperature emission lines (C II, Si IV, C IV, N V, O V, etc.) and the bulk of the flux in the low-temperature emission lines (Mg II, O I, Si II, etc.) are from the late-F–type secondary, *not* from the primary. We feel that the presence of very different outer atmospheres around two ostensibly very similar stars within the same system provides a crucial test of our understanding of the physical basis for chromospheric and coronal phenomena. To preview our conclusions, we believe that the key to the Capella dichotomy is stellar rotation.

In § II we summarize stellar parameters for Capella Aa and Ab, and an evolutionary scenario for the system. We describe our ultraviolet spectra and previous observations of Capella in § III, including line identifications, line fluxes, and estimates of the relative contribution of each star to the composite line profiles. In § IV we discuss the importance of rotation and consider possible transition-region models for the Capella secondary.

II. STELLAR PARAMETERS FOR CAPELLA

a) Astrometry

The two components of Capella have nearly equal masses ($\mathfrak{M}_{Aa} \approx 2.7\,\mathfrak{M}_\odot$; $\mathfrak{M}_{Ab} \approx 2.6\,\mathfrak{M}_\odot$); the binary orbit is circular with a period of 104 days and an inclination of 137°; and the system parallax is 0.″076, which corresponds to a distance of 13.2 pc (Batten, Fletcher, and Mann 1978; Heintz 1975). The orbital parameters determined spectroscopically by Finsen (1975) and others have been verified by direct interferometric measurements (Blazit *et al.* 1977).

b) Optical Spectroscopy

Optical spectra of Capella are somewhat unusual. First, weak and strong lines of the primary are readily visible, but only strong lines of the secondary are prominent in the composite spectrum (Struve and Kung 1953). Wright (1954) pioneered the study of Capella by using mechanical subtraction of spectrogram tracings to isolate the secondary spectrum. He concluded, from comparisons with standard stars, that the Capella primary is an ordinary giant of spectral type late G, while the secondary is somewhat hotter, probably a late F or early G giant. The diffuse appearance of weak features in the Ab spectrum has been attributed to either rapid rotation (Herbig and Spaulding 1955; Wallerstein 1966; Boesgaard 1971) or enhanced turbulence (Struve and Kung 1953; Franklin 1959).

The second unusual characteristic of the Capella spectrum is the presence of a prominent lithium absorption feature at 6708 Å, that follows the radial velocities of the secondary, but only weak lithium absorption in the primary spectrum (Wallerstein 1966; Boesgaard 1971). This suggests that the Capella primary has lost most of its primordial surface lithium by deep mixing, whereas the secondary has not. Iben (1965) proposed an evolutionary scenario to explain the peculiarities of the Capella system. He suggested that both components were initially late B or early A stars on the main sequence. Subsequent evolution carried the slightly more massive primary horizontally across the H-R diagram, up to helium flash at the tip of the giant branch, and back down toward the zero-age main sequence (ZAMS). Meanwhile, the somewhat less massive secondary only recently has evolved away from the ZAMS and has not yet developed a deep enough convection zone to significantly deplete the primordial lithium in its photosphere. Iben's evolutionary picture explains in a natural way how the binary companions of nearly similar mass can be found in nearly the same location in the H-R diagram, yet have vastly different surface lithium abundances and rotation rates (see § III).

c) Photometry

The visual luminosity difference between the Capella primary and secondary is small. Wright (1954) estimated $\Delta V \equiv V_{Ab} - V_{Aa} \simeq +0.25$ mag by adding pairs of F and G giant spectra to fit the composite spectrum. His result is consistent with interference fringe contrasts in speckle pictures of Capella which suggest that ΔV is less than 1 mag (Labeyrie 1975).

High-quality photometry is available for Capella (Johnson *et al.* 1966), including far-ultraviolet colors from *OAO 2* (Code and Meade 1979). We use the measured photometric color indices to estimate effective temperatures, radii, luminosities, and other fundamental parameters for each star.

d) Derived Stellar Parameters

i) *Component* $(B - V)$ *Colors*

Because the Capella secondary is somewhat hotter than the primary, ultraviolet colors of the system will be dominated by the former while infrared colors will be dominated by the latter. We chose $(B - V)$ as a transfer color and established linear relationships between the *OAO 2* ultraviolet index $(C_{1910\text{Å}} - V)$, and $(B - V)$, and between the infrared index $(V - L)$ and $(B - V)$. Using these empirical relationships we constructed curves in a color-color diagram which were the loci of $(B - V)_{Aa}$, $(B - V)_{Ab}$ points that reproduced the observed system ultraviolet or infrared color index for a given V-magnitude difference. The intersection point of the UV and IR color-color

loci is the $(B-V)_{Aa}$, $(B-V)_{Ab}$ pair that reproduces the UV *and* IR system colors for the particular ΔV. For example, with $[C_{1910}-V]_* = +5.29$ mag, $(V-L)_* = +1.95$ mag and $\Delta V = 0.25$ mag, we find $(B-V)_{Aa} \approx +0.90$ mag and $(B-V)_{Ab} \approx +0.60$ mag. These values systematically change by $\Delta(B-V) = \pm 0.03$ mag, ± 0.01 mag for the primary and secondary, respectively, with a ± 0.25 mag change in ΔV. The component $(B-V)$ colors for $\Delta V = +0.25$ mag correspond to spectral types G6 for the primary and F9 for the secondary, at luminosity class III. These spectral types are nearly identical to those proposed by Wright (1954) based on optical spectra of the system.

ii) $T_{\rm eff}$, *B.C.*, *L*, *R*

We estimated component effective temperatures using a composite $T_{\rm eff}-(B-V)$ relation for dwarfs and giants (Johnson 1966), normalized to the solar effective temperature 5770 K at $(B-V)_\odot \approx 0.65$ mag (Flannery and Ayres 1978; Barry, Cromwell, and Schoolman 1978). We find from the individual Capella colors, $T_{\rm eff}^{\rm Aa} \approx 5100$ K and $T_{\rm eff}^{\rm Ab} \approx 6000$ K. The uncertainties in $(B-V)$ imply a roughly ± 100 K uncertainty in the derived effective temperatures, but systematic errors could, of course, be larger. We also estimated differential bolometric corrections relative to the Sun based on a B.C.–$(B-V)$ relationship. The bolometric corrections, the stellar distance modulus, and the solar absolute visual magnitude of $M_V^\odot \approx +4.81$ mag were used to convert the apparent magnitudes of the Capella stars, $V_{Aa} = +0.72$ mag and $V_{Ab} = +0.97$ mag, to luminosities relative to the Sun, $L_*/L_\odot$. Finally, stellar radii were derived from the estimated luminosities and effective temperatures. The system and component parameters are summarized in Table 1.

TABLE 1

SYSTEM AND COMPONENT PARAMETERS FOR CAPELLA

Parameter	System[a]	Primary (Aa)[b]	Secondary (Ab)[b]
d (pc)	13.2	...	...
P (days)	104	...	...
Age (yr)	3.5×10^8[c]	...	...
V (mag)	+0.08	+0.72	+0.97
$[C_{1910}-V]$ (mag)	+5.29[d]	...	...
$(V-L)$ (mag)	+1.95	...	...
$(B-V)$ (mag)	+0.80	+0.90	+0.60
Spectral type	...	G6 III	F9 III
$T_{\rm eff}$ (K)	...	5100	6000
$L/L_\odot$	...	82	59
$R/R_\odot$	...	11.6	7.1
$\mathfrak{M}/\mathfrak{M}_\odot$	...	2.67[a]	2.55[a]

[a] Batten, Fletcher, and Mann 1978, unless otherwise noted.

[b] This work, with $\Delta V \equiv V_{Ab} - V_{Aa} = +0.25$ mag.

[c] Based on Iben 1967 tracks, intervals 1–5 for 2.6 $\mathfrak{M}_\odot$ star (interpolated).

[d] Code and Meade 1979.

III. ULTRAVIOLET OBSERVATIONS

a) *Work Previous to IUE*

Capella has been observed spectroscopically in the vacuum ultraviolet by *Copernicus* at high resolution in the 1000–1300 Å region (Dupree 1975), by a Johns Hopkins rocket spectrometer at moderate resolution between 1150 and 1600 Å (Vitz *et al.* 1976), and by both *Copernicus* (Dupree 1976) and the BUSS balloon experiment (Kondo, Morgan, and Modisette 1976; Kondo *et al.* 1979) at the Mg II λ2800 resonance doublet. Capella's broad-band energy distribution has been measured by *OAO 2* down to 1900 Å (Code and Meade 1979) and by TD1 down to 1600 Å (Jamar *et al.* 1976).

Copernicus detected significant emission from the resonance lines of O VI λ1032, Si III λ1206, H I Lα (1216 Å), and N V λ1239 Å (Dupree 1976). In addition to the *Copernicus* detections, the Vitz *et al.* (1976) rocket experiment observed strong emission from the following: the 1175 Å multiplet of C III, the 1305 Å resonance triplet of O I, the resonance doublets of C II λ1335, Si IV λ1400, and C IV λ1550, and the Si II doublet near 1265 Å.

Capella has also been detected as a bright soft X-ray source in several rocket and satellite experiments (see Holt *et al.* 1979; Cash *et al.* 1978, and references therein). The soft X-rays are presumed to be emitted by a stellar analog of the solar corona. However, the inferred plasma temperature is hotter than that of the solar corona (10^7 K vs. 2×10^6 K), and the coronal emission measure, EM $\approx \int n_e^2 dV$, is about 10^4 times that of the average Sun. In addition, there is evidence from *ANS* (Mewe *et al.* 1975) and *HEAO 1* (Cash *et al.* 1978) that the X-ray emission is somewhat variable. Capella shares many X-ray properties in common with the short-period RS CVn-type binary systems (Walter, Charles, and Bowyer 1978), and it tentatively has been identified as a long-period member of the class (Hall 1976).

b) *IUE Observations*

Echelle spectra of Capella in the long-wavelength (2000–3200 Å) and short-wavelength (1150–2000 Å) regions were obtained during *IUE* scientific commissioning operations, and are described by Linsky *et al.* (1978). Subsequent observations taken in 1978 April, May, and August are summarized in Table 2. Coverage of the binary orbit in the recent data is limited to the velocity crossing at 52 days and to several days near the elongation at 78 days, when the radial velocity separation is at maximum. We restrict our consideration to the recent observations, which are of much higher quality than those obtained during the commissioning phase.

i) *Short-Wavelength, Low-Dispersion Spectra*

Five low-dispersion ($\sim$6 Å FWHM) spectra of the short-wavelength region in Capella were taken on 1978 August 15. Three were through the large aperture

TABLE 2

SUMMARY OF CAPELLA OBSERVATIONS

Image[a]	Dispersion[b]	Aperture[c]	Exposure Time	Date (1978)	Begin UT	Orbital Phase[d] (days)
SWP 1304	HI	S	16^m	Apr 3	12^h03^m	52
SWP 1305	HI	S	120^m	Apr 3	13 23	52
LWR 1276	HI	S	72^s	Apr 3	16 29	52
LWR 1277	HI	S	3^m	Apr 3	17 47	52
SWP 1454	HI	S	90^m	May 1	17 39	81
SWP 2296	LO	L	6^m	Aug 15	03 09	82
SWP 2296	LO	S	6^m	Aug 15	03 22	82
LWR 2077	HI	L	2^m	Aug 15	03 41	82
SWP 2297	LO	L	90^s	Aug 15	04 46	82
SWP 2297	LO	S	90^s	Aug 15	04 56	82
LWR 2078	HI	L	40^s	Aug 15	05 07	82
SWP 2298	LO	L	30^m	Aug 15	05 55	82
SWP 2299	HI	L	180^m	Aug 15	07 16	82
SWP 2352	HI	S	60^m	Aug 21	13 00	88

[a] SW = 1150–2000 Å; LW = 2000–3200 Å; P = prime camera; R = redundant camera.

[b] HI = echelle mode; LO = low dispersion.

[c] S = 3″ diameter aperture; L = 10″ × 20″.

[d] Phase O days refers to the conjunction with the Aa component in front.

(10″ × 20″) and two were through the small aperture (3″ diameter). Exposure times ranged from 90 seconds to 30 minutes to compensate for the limited dynamic range of the vidicon cameras compared with the diversity in line and continuum emission strengths.

The large- and small-aperture exposures were individually corrected for scattered light (see Paper III) and were registered to a common wavelength scale using the positions of the prominent emission features O I λ1305, C II λ1335, and C IV λ1550. The five spectra were then co-added to form a cumulative exposure. Regions of the individual spectra that were saturated or affected by reseau marks were omitted from the superposition, and the cumulative exposure times for those intervals were reduced accordingly. Because an uncertain fraction of the stellar image is transmitted by the small aperture, typically only 50%, an effective exposure time was determined for the two small-aperture spectra by comparing the signal levels in unsaturated continuum regions of small- and large-aperture spectra having the same uncorrected exposure time (see Table 2). The composite spectrum is the sum of the five independent exposures in intrinsically faint regions, but includes only the shortest exposures in the bright continuum region longward of 1900 Å and in the core of the 1216 Å Lα feature. Finally, the composite spectrum was divided by the cumulative exposure time and multiplied by the inverse sensitivity curve S_λ^{-1} for the short-wavelength prime spectrograph (Bohlin *et al.* 1979).[4] The resulting spectrum is calibrated in absolute flux units at the Earth. These data are compared in Figure 1 with the integrated disk quiet-Sun spectrum (Rottman 1978) as it would appear at a distance of 1 pc, degraded by the approximate 6 Å FWHM resolution of the *IUE* short-wavelength, low-dispersion mode.

Unlike the solar-type stars α Centauri A (G2 V) and B (K1 V) described in Paper III, Capella's ultraviolet spectrum is qualitatively and quantitatively different from that of the quiet Sun. The high-temperature ($T \approx 10^5$ K) lines N V λ1240, Si IV λ1400, and C IV λ1550 are enhanced over their solar counterparts by a factor of about 20. In addition, the relative strengths of low- and high-temperature lines appear to be quite different in the Sun and Capella. For example, the O I λ1305 triplet feature in Capella is brighter than the neighboring C II λ1335 doublet, whereas C II is brighter than O I in the Sun (see also Vitz *et al.* 1976). In addition, the C IV λ1550 doublet is several times brighter than the C I multiplet near 1657 Å in Capella, whereas these carbon features are essentially the same strength in the Sun.

Finally, the continuum region longward of 1700 Å is brighter, and the continuum slope is flatter, in Capella than in the Sun (at 1 pc). Virtually all of the continuum flux in this region is from the hot secondary.

ii) *Short-Wavelength Line Identifications*

Table 3 lists the prominent emission features in the low-dispersion, composite spectrum of Capella and tentative line identifications. References to the quiet- and active-Sun line lists which form the basis for our identifications are given in Paper III.

Wherever possible, we have used echelle mode spectra in the short-wavelength region to corroborate the low-dispersion identifications. The high-dispersion

[4] At present, the absolute flux calibration of the SWP camera is uncertain owing to an error in the intensity transfer function (Holm 1979). However, we expect such errors to be minimal for the low-resolution, composite spectrum of Capella, since the most heavily weighted images in the superposition are the *deepest* exposures. These typically have flux-number levels far above the affected region. Nevertheless, we are currently implementing the correction algorithm and will provide updated line fluxes if there are any changes.

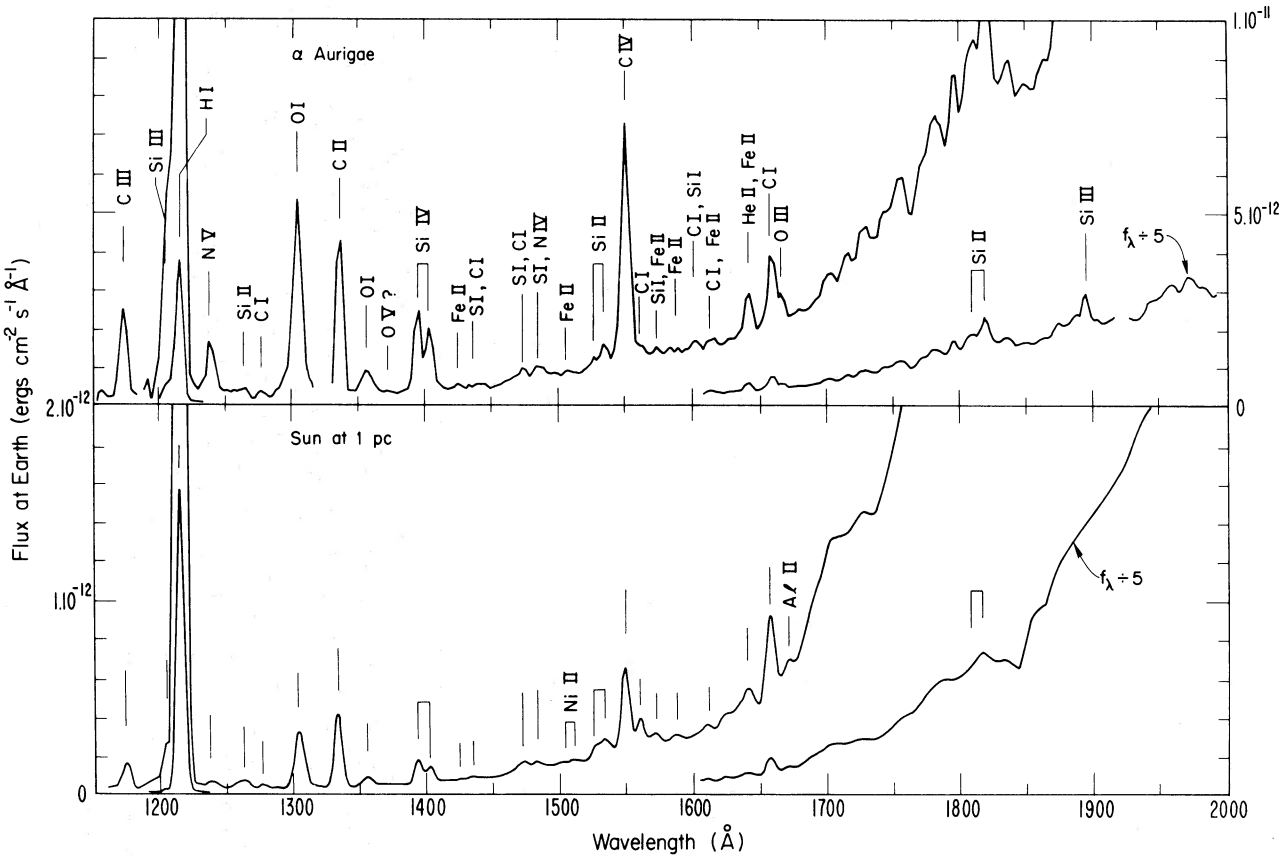

FIG. 1.—Comparison of *IUE* composite short-wavelength spectrum of Capella with the integrated-disk quiet-Sun spectrum as it would appear at a distance of 1 pc and degraded to the approximate 6 Å FWHM resolution of the *IUE* low-dispersion mode. The solar and stellar spectra can be compared directly on the apparent flux scale (i.e., ergs cm^{-2} s^{-1} at the Earth), because the Sun at 1 pc would subtend a solid angle comparable to that of the combined components of Capella. Gaps in the Capella spectrum are regions affected by reseau marks.

spectra can provide accurate line positions, separate blends, and indicate line strength ratios in multiplets. These data are particularly useful longward of 1700 Å. There, except in a few cases such as the Si II triplet near 1815 Å and Si III λ1892, it is difficult to distinguish true emission features from mere gaps between strong absorption lines in the low-dispersion data. Several tentative identifications of Fe II emission in the low-dispersion spectrum were rejected on this basis.

iii) *Low-Dispersion Integrated Fluxes*

Also listed in Table 3 are absolute fluxes for the prominent emission features in the low-dispersion data. These fluxes refer to the emission above an estimated background to correct for the photospheric continuum of the secondary. The background level was interpolated between minima of the energy distribution away from the strong emission features. Nevertheless these minima may be contaminated by weak emission lines, and the measured fluxes may be slightly underestimated as a result. Finally, Table 3 includes fluxes of individual lines in blends obtained from the relative integrated intensities in the high-dispersion data, and the absolute flux for the blend in the low-dispersion data.

iv) *Echelle Mode Spectra, Long-Wavelength Region*

The intrinsically bright 2000–3200 Å region of the spectrum contains the Mg II *h* (2803 Å) and *k* (2796 Å) and Mg I λ2852 resonance lines formed in the chromosphere and upper photosphere, but no prominent lines formed at temperatures hotter than 10^4 K. The optically thick Mg II *h* and *k* emission cores are important sources of radiative cooling in the middle chromosphere (Linsky and Ayres 1978), and may provide useful constraints on pressures in the upper chromosphere at the chromosphere-corona interface.

Our best spectrum of the Mg II doublet is illustrated in Figure 2. These data are from a 40 second large-aperture exposure (image LWR 2078) taken on 1978 August 15 at orbital phase 82 days, 4 days past elongation. The Mg II spectrum was taken during the same observing shift as the five low-dispersion, short-

TABLE 3

LINE IDENTIFICATIONS

Approximate Wavelength (Å) (low dispersion)	f_{total} (10^{-12} ergs cm^{-2} s^{-1})	Identification	Approximate Wavelength (Å) (high dispersion)[a]	f_l (10^{-12} ergs cm^{-2} s^{-1})
1175	18	C III (4)[b]	(1175)[c]	...
1216	310[d]	H I (1) Lα	(1216)	290
		Si III (2)	1206.5	20:[e]
		O V	1218.3:	3:
1238	13	N V (1)	1238.8	8.6
		N V (1)	1242.9	4.4
1265	2.8:	Si II (4)	...	...
1277	1.8:	C I	...	...
1304	49	O I (2)	1302.2	14
		O I (2)	1304.9	19
		O I (2)	1306.0	17
1336	27	C II (1)	1334.7	12
		C II (1)	1335.7	15
1355	7.6	O I (1) + C I	...	...
1371	1.1:	O V (7)	1371.1:	...
1395, 1403	26	Si IV (1)	1393.8	15
		O IV	1401.0:	2.1:
		Si IV (1)	1402.8	7.7
		O IV	1404.7:	1.2:
1424	1.4:	Fe II (47) + S I	...	...
1432	0.6:	C I (65) + S I	...	...
1438	2.0:	S I (5)?	...	...
1472	3.4:	S I (4, 3)	...	...
1483	4.5:	S I (4, 3)	...	...
		N IV	1486.5:	...
1505, 1511	1.5:	Fe II, Ni II (6), C I	...	...
1525, 1533	4.9:	Si II (2)	...	...
1549	44	C IV (1)	1548.2	28
		C IV (1)	1550.8	16
1561	2.4:	C I (3)	...	...
1573	1.2:	Si I + Fe II	...	...
1583, 1588	2.2:	Fe II (44)	...	...
1595, 1602	2.1:	Si I + C I	...	...
1614	2.6:	C I + Fe II	...	...
1626	0.7:	Fe II (43)? + Si I?	...	...
1641	7.2	He II (12) + Fe II	1640.5	...
1659, 1666	16	C I (2)	(1657)	12
		O III	1660.7:	0.9:
		O III	1666.0:	3.2:
1809, 1577	51:	Si II	1808.0	8
		Si II	1817.0	43
		Si II	1817.4	
1894	36:	Si III (1)	1892.0	26[f]
		C III	1908.8	8[f]

[a] Based on spectra obtained at velocity crossing; wavelengths in center of mass frame.

[b] Multiplet number.

[c] Parentheses indicate uncertain wavelength owing to very broad feature or multiplet structure.

[d] No correction for interstellar absorption or geocoronal emission.

[e] Colons indicate uncertain quantities.

[f] Derived from echelle data using 1900 Å region continuum flux estimated from low-dispersion spectrum.

wavelength images described in § III*b*[ii] above, and 2 hours before a long-exposure, echelle spectrum of the short-wavelength region (SWP 2299).

At orbital phase 82 days, the Capella primary is blueshifted relative to the system center of mass velocity ($V_0 = +29.5$ km s^{-1}; Batten, Fletcher, and Mann 1978), while the secondary is redshifted. The velocity separation of the two stars is of order 50 km s^{-1}. The doubling of the Mg II *h* and *k* features resulting from the velocity splitting is clearly seen in Figure 2, even though the intrinsic widths of the Mg II features are too large to permit the complete separa-

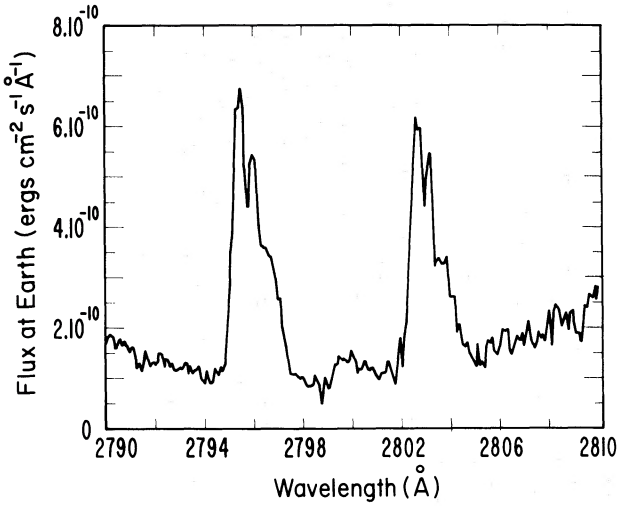

FIG. 2.—Echelle mode profiles of the Mg II λ2800 resonance doublet taken near maximum velocity separation of the binary components. The doubling of the *h* (2803 Å) and *k* (2796 Å) profiles is clearly apparent. At that orbital phase (82 days), the Capella primary is blueshifted relative to the secondary.

tion of the component profiles. Note that the short-wavelength emission edges of both *k* and *h* are much steeper than the long-wavelength edges, and that the visible portion of the Ab *k* line appears to be smooth and rounded compared with the sharp double reversal of the Aa core.

The LWR images taken during the velocity crossing at phase 52 days (1978 April 3) are of much poorer quality than the data illustrated in Figure 2, and, unfortunately, are not suitable for analysis. However, the *h* and *k* profiles in LWR 1276 appear to be single and the emission peaks are symmetric. A similar behavior is seen in *Copernicus* profiles of *k* recorded close to velocity crossing at phase 50 days (Dupree 1976, her Fig. 1). We have also examined BUSS spectra of the Capella Mg II doublet. Initial observations of *h* and *k* on 1975 March 14/15 at phase 81 days (Kondo, Morgan, and Modisette 1976) appear to be asymmetric in the same sense as our *IUE* phase 82 days profiles (Fig. 2), although the spectral resolution of the early BUSS echelle was lower than that of *IUE*. Capella was again observed by BUSS on 1976 September 17 (Kondo *et al.* 1979) with a higher-resolution spectrograph. These data were obtained at orbital phase 9 days, when the secondary was *blueshifted* relative to the primary by about 27 km s^{-1}. The BUSS Mg II profiles are essentially mirror images of those in Figure 2. The long-wavelength emission edges of *h* and *k* in the BUSS spectra are steeper than the short-wavelength edges, and the short-wavelength emission peaks are weaker than their long-wavelength counterparts. (The emission peak asymmetry is reversed in the 1978 August 15 spectra.) A phase-dependent emission peak asymmetry can be explained simply if the intrinsic Mg II double reversal of the primary is nearly symmetric (as it appears to be in image LWR 1276 taken at velocity crossing) and if the secondary has a weak, but present, k_3 self reversal. As the Ab profile shifts back and forth relative to the Aa profile, whichever of the sharp Aa peaks coincides with the Ab k_3 feature will weaken relative to the other peak. Note, however, that a qualitatively similar behavior would result if the k_3 feature seen in the phase 82 days profile is largely interstellar (Böhm-Vitense 1980). Either effect would compromise the conventional interpretation of Mg II emission peak asymmetries in terms of chromospheric bulk motions (Dupreee 1976).

Although a standard absolute calibration is not yet available for the *IUE* LWR echelle mode data, it is possible to estimate a flux scale by comparing the Capella spectra with observations of a calibration star (η UMa, B3 V). Basri and Linsky (1979) have described that procedure and we adopt their Mg II region calibration here. The inferred integrated flux for *k*, 7×10^{-10} ergs cm^{-2} s^{-1} at the Earth, is similar to that of *h*.

v) *Echelle Mode Spectra, Short-Wavelength Region*

The 1150–2000 Å short-wavelength region in cool stars like Capella and the Sun is rich in strong emission features from a variety of species formed in the middle chromosphere ($T \approx 6 \times 10^3$ K), the upper chromosphere ($T \approx 2 \times 10^4$ K), and the stellar analog of the solar transition region ($T \approx 10^5$ K).

Middle chromosphere ($T \approx 6 \times 10^3$ K).—The important features formed at middle-chromosphere temperatures are multiplets of O I λλ1302, 1305, 1306; C I λλ1560, 1657; and Si II λλ1808, 1816, 1817. All of these features appear in the best of the five echelle mode spectra, namely, image SWP 1305 taken at the phase 52 days velocity crossing, and image SWP 2299 obtained 4 days past elongation, at phase 82 days.

Profiles of the O I features near the phase 52 days velocity crossing are reasonably symmetric. Near elongation, the O I features become broader and asymmetric in the same sense as the Mg II resonance line cores. The strength of O I in Capella may be related indirectly to the large Lα flux, since the triplet features in cool stars can be pumped by Lβ through a Bowen fluorescence mechanism (Haisch *et al.* 1977). In fact, cool giants tend to exhibit roughly a factor of 5 enhanced O I surface fluxes compared with dwarf stars of similar effective temperature and chromospheric activity levels (Ayres, Marstad, and Linsky 1980).

The C I multiplets at 1560 and 1657 Å are more difficult to interpret than the O I triplet because several individual features contribute to the overall blend (Shine, Lites, and Chipman 1978). It is not clear, for example, whether the small changes observed in the 1657 Å emission envelope between velocity crossing and elongation are a result of radial velocity shifts or genuine changes in relative line strengths within the multiplet itself.

The Si II triplet exhibits a similar behavior to that of the O I triplet. The Si II lines are narrower than those formed at higher temperatures (see below), they are symmetric at velocity crossing, and they are asymmetric near elongation in the same sense as the Mg II emission cores. Tripp, Athay, and Peterson (1978) have described the formation of the Si II features in the solar chromosphere, and Simon, Kelch, and Linsky (1980) have discussed the formation of these lines in ϵ Eri (K2 V). They both conclude that the triplet features are formed primarily in the middle chromosphere, although the presence of temperature plateaus in the upper chromosphere can contribute significantly to the Si II core intensities.

Upper chromosphere ($T \approx 2 \times 10^4$ K).—Prominent emission features formed in the upper chromosphere include H I Lα, He II λ1640,and C II $\lambda\lambda$1335, 1336.

The hydrogen resonance line is potentially the most important of these as a diagnostic, because Lα radiative cooling very likely controls the thermal structure of the upper chromosphere, and because the extensive Stark-broadened damping wings of Lα can be used to map the chromospheric temperature structure from the 2×10^4 K level down to the middle chromosphere itself (Basri *et al.* 1979). In practice, however, the core of Lα is almost entirely obliterated by interstellar H I extinction, and much of the extensive damping wings is too faint to be observed reliably by *IUE*.

The He II Balmer α line (1640 Å) exhibits a similar behavior to that of the O I and Si II triplets. However, the formation mechanism for the He II subordinate line is a subject of dispute (e.g., Linsky 1977); consequently, the diagnostic value of He II λ1640 remains to be established. Furthermore, the He II emission is contaminated by an uncertain contribution from Fe II λ1640 (Kohl 1977).

The C II doublet at 1335, 1336 Å is formed at temperatures near 2×10^4 K, and exhibits the characteristics of the 10^5 K lines, namely, the features are broad and the line shapes are not obviously different near elongation compared with velocity crossing.

Transition region ($T \approx 10^5$ K).—Prominent features formed at transition-region temperatures include the resonance doublets of Si IV $\lambda\lambda$1394, 1403; C IV $\lambda\lambda$1548, 1551; and N V $\lambda\lambda$1239, 1243. Less prominent, but important high-temperature features include the 1218 Å and 1371 Å intercombination lines of O V and the 1487 Å intercombination line of N IV. Prominent features formed at somewhat cooler temperatures include the 1175 Å multiplet of C III; the Si III resonance line at 1206 Å; and intercombination lines of O III $\lambda\lambda$1661, 1666; Si III λ1892; and C III λ1909. All of these features appear in the deepest echelle mode exposures (SWP 1305 and SWP 2299), and all but O V λ1218, which is blended with Lα, are visible in the low-dispersion composite spectrum.

The high-temperature lines share three important characteristics in common. The features are broad (FWHM $\gtrsim 100$ km s^{-1}), they are relatively symmetric at velocity crossing *and* near elongation, and they appear to follow the radial velocities of the secondary star.

Coronal lines ($T \gtrsim 10^6$ K).—We searched in our SWP spectra for the strongest forbidden transitions seen in the solar coronal spectrum: Fe XII $\lambda\lambda$1242, 1349; Si VIII λ1446; and Fe XI λ1467 (Sandlin, Brueckner, and Tousey 1977). However, none of these features was detected even in the deepest echelle mode exposures, and the resolution of the low-dispersion mode does not allow unambiguous identification of weak features. We conclude that high-resolution observations of greater sensitivity are needed to detect the presence of very high excitation lines in the Capella spectrum.

Summary of high-resolution spectra at velocity crossing and near elongation.—Figures 3 and 4 depict the high-dispersion spectra of Capella at velocity crossing and near maximum velocity separation.

Figure 3 illustrates Lα profiles from four of our five echelle mode exposures of the short-wavelength region. The fifth image, SWP 2299, was heavily exposed, and only the extreme core and far wings of Lα are unsaturated.

Listed in the upper left-hand corners of each panel in Figure 3 are "equivalent exposure times" t (in kiloseconds). These are the approximate exposure times for *large-aperture* images required to produce comparable DN levels at Lα. The ratios of the equivalent to actual exposure times, typically 0.5, are measures of the effective transmission of the small slot for the particular observations.

The velocity scales are relative to the heliocentric center-of-mass (COM) velocity of the system (§ II). We obtained the COM velocity scales by correcting for the projected ecliptic motion of the Earth toward Capella at the times of observation, but we did not take into account a possible spacecraft motion of ± 4 km s^{-1}. The corrected velocity scales of images SWP 1304, 1305, and 1454 appear to contain systematic errors compared with the most recent, small-aperture exposure SWP 2352, which was taken expressly to provide an accurate wavelength scale. We established a COM velocity scale for the phase 52 days image SWP 1305 according to the centroids of the chromospheric features O I $\lambda\lambda$1305, 1306 and Si II λ1808.[5] The dispersion among the three independent velocity centroids is of order ± 2 km s^{-1}, which is comparable to the internal consistency cited

[5] In practice, a line centroid is the mean of five separate measurements evenly spaced between the 30% and 70% residual flux levels. The errors cited (in Table 4, e.g.) are the formal 1 σ standard deviations obtained from the centroid measurement set of each line. These errors are an indication of how accurately a line position can be measured on the given velocity scale by the simple centroid technique, rather than an indication of the overall absolute accuracy of the velocity scale itself. However, the *internal consistency* of the SWP velocity scale is well established (*IUE Newsletter*, No. 2); consequently any *relative* velocity shifts quoted should be reasonably accurate.

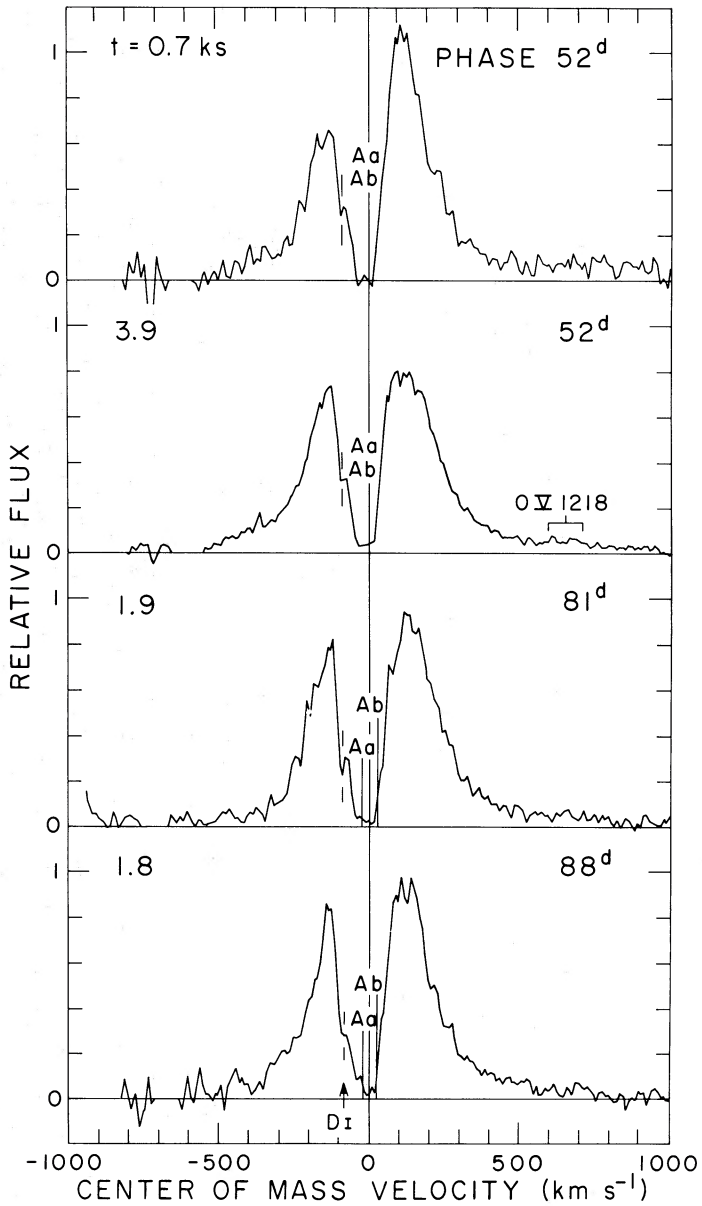

FIG. 3.—Echelle mode profiles of H I Lα taken at velocity crossing and near elongation. The extreme core of the intrinsic stellar feature is largely obliterated by interstellar Lα absorption and geocoronal emission. A weak absorption feature near -100 km s^{-1} attributed to interstellar *deuterium* Lα is also seen. The positions of the primary and secondary relative to the system center of mass velocity at each orbital phase are indicated. Equivalent exposure times "t" (see text) for each image are also given.

for small-aperture measurements of sharp interstellar features in hot-star spectra (*IUE Newsletter*, No. 2). However, the apparent zero point of the SWP 1305 velocity scale is redshifted by 70 km s^{-1} relative to the zero implied by the O I + Si II centroids (note that $V_{Aa} = V_{Ab} = V_{COM}$ at phase 52 days). If we adopt the O I + Si II velocity zero, we find excellent agreement between the positions of the interstellar Lα absorption cores of SWP 1305 and SWP 2352. We next registered SWP 1304 and 1454 to the SWP 1305–2352 velocity scale according to the individual interstellar Lα features. The velocity corrections were $+65$ km s^{-1} for SWP 1304 (vs. $+70$ km s^{-1} for SWP 1305) and -10 km s^{-1} for SWP 1454. The velocity scale of the large-aperture image SWP 2299 is consistent with that of SWP 2352, and required no correction.

Finally, we checked the internal consistency of the velocity scale registrations by comparing the positions of the well-known interstellar D I Lα absorption features in each exposure. The mean D I velocity for the four small-aperture exposures is -10 ± 2 km s^{-1}

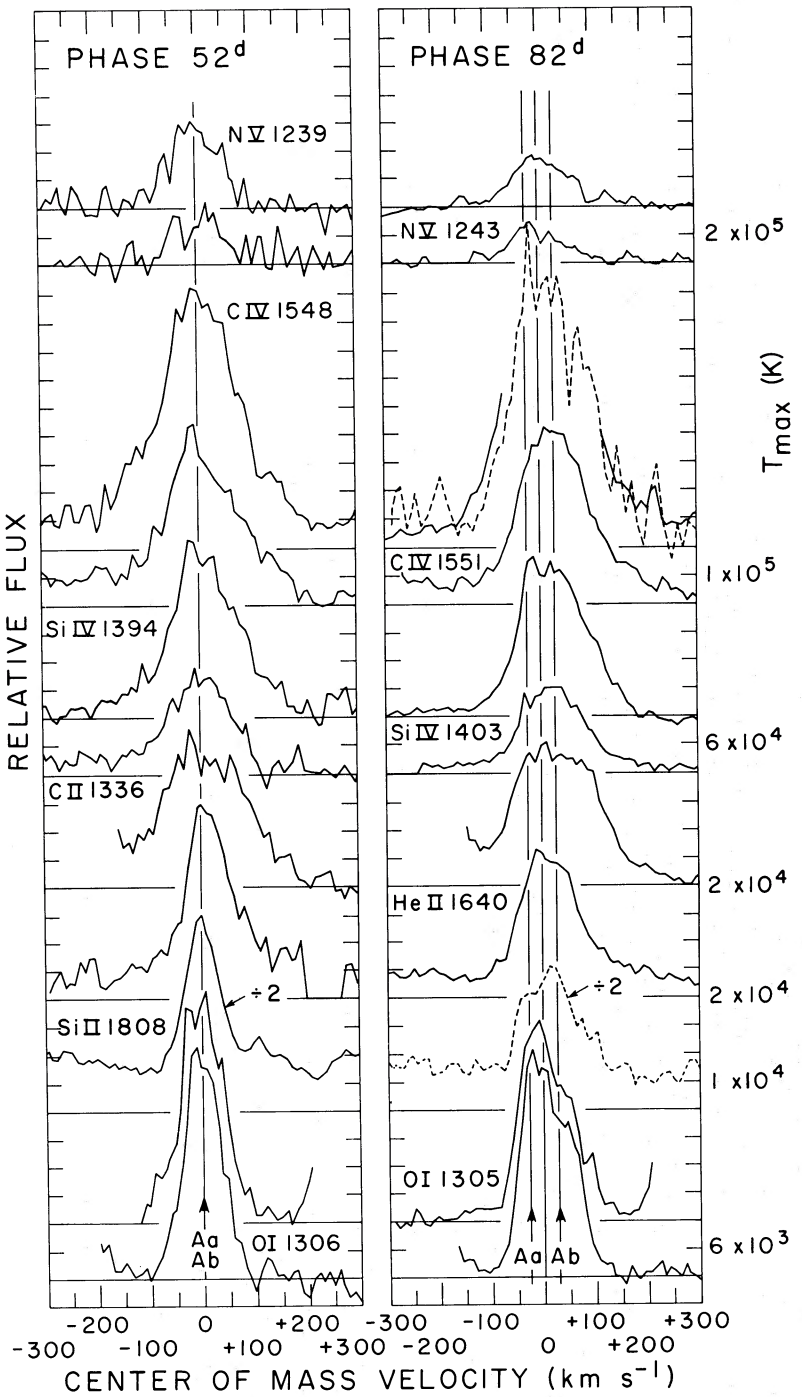

FIG. 4.—Comparison of echelle mode profiles of prominent short-wavelength emission features at velocity crossing and near elongation. The profiles are ordered from bottom to top in a sequence of increasing formation temperature. The velocities of Capella Aa and Ab relative to the system center of mass at the two orbital phases are indicated. The horizontal lines are zero levels for the individual profiles. Sections in two of the profiles (He II: 52 days; N V λ1243: 82 days) affected by reseau marks have been assigned zero flux. Note that the high-temperature lines exhibit no large velocity shifts relative to the low-temperature features at velocity crossing (left-hand panel). Also note the doubling of the low-temperature lines near elongation (right-hand panel), whereas the high-temperature profiles remain symmetric and shift to the red following the radial-velocity motion of the Capella secondary. The profiles in the left-hand panel are from image SWP 1305. The profiles in the right-hand panel are from SWP 2299 (*solid curves*), with the exceptions of C IV λ1548 and Si II λ1808 which are from SWP 1454 (*dashed curves*). (The unsaturated portion of the SWP 2299 C IV λ1548 profile is indicated by the truncated solid curve.)

TABLE 4

PROPERTIES OF SELECTED ULTRAVIOLET LINES AT VELOCITY CROSSING AND NEAR-ELONGATION

TRANSITION	REST WAVELENGTH[a] (Å)	APPROXIMATE TEMPERATURE[b] OF FORMATION (K)	WEIGHT[d]	PHASE 52 days (SWP 1305) Centroid Velocity[c] (km s^{-1})	PHASE 52 days (SWP 1305) FWHM (km s^{-1})	PHASE 82 days (SWP 2299) Centroid Velocity[c] (km s^{-1})	PHASE 82 days (SWP 2299) FWHM (km s^{-1})
H I Lα	1215.67	10^4	...	$+15 \pm 3$	460	15 ± 7[e]	450[e]
Interstellar D I Lα	1215.34	...	...	-10	...	-8[e]	...
N V 1239	1238.82	2×10^5	2	$+1 \pm 5$	130	13 ± 4	133
N V 1243	1242.80	2×10^5	1	$+1 \pm 4$	103	2 ± 8	106
O I 1305	1304.86	6×10^3	...	$+1 \pm 2$	88	2 ± 7	116
O I 1306	1306.03	6×10^3	...	-1 ± 2	77	6 ± 7	120
C II 1336	1335.71	2×10^4	4	$+9 \pm 3$	206	28 ± 2	190
Si IV 1394	1393.76	6×10^4	4	$+14 \pm 5$	143	25 ± 6	148
Si IV 1403	1402.77	6×10^4	2	$+1 \pm 3$	138	23 ± 3	140
C IV 1548	1548.20	10^5	8	$+9 \pm 4$	157	27 ± 5[e]	165[e]
C IV 1551	1550.77	10^5	4	$+7 \pm 9$	130	28 ± 3	141
He II 1640	1640.40	2×10^4 (?)	...	$+15 \pm 6$	102	10 ± 2	118
Si II 1808	1808.01	10^4	...	$+1 \pm 1$	64	8 ± 5[e]	115[e]
Weighted average				$+8 \pm 4$[f]		$+25 \pm 6$[g]	

[a] Cohen, Feldman, and Doschek 1978.

[b] White and Lemaire 1976.

[c] Velocities are defined relative to system center of mass (see § III*b*[v]).

[d] Relative TR line strengths used in velocity centroid weighting.

[e] From image SWP 1454 (phase 81 days).

[f] ($V_{Aa} = V_{Ab} = 0$).

[g] ($V_{Aa} = -26$; $V_{Ab} = +27$).

relative to the rest wavelength of the D I feature in the COM velocity frame. The dispersion of the individual values about the mean is comfortingly small, and the implied interstellar neutral hydrogen radial velocity, $V_{H\,I} \approx 20$ km s^{-1}, is compatible with the values cited by Dupree, Baliunas, and Shipman (1977) based on *Copernicus* measurements of the Capella Lα core.

Having established the COM velocity scales, we next determined centroid velocities and FWHMs for the individual Lα emission profiles. Curiously, we find essentially no variation of the centroid velocities and line widths with orbital phase (Table 4). We estimate from the four Lα profiles, weighted according to the equivalent exposure times, that $V_{COM}(L\alpha) = 14 \pm 2$ km s^{-1} and FWHM $= 440 \pm 20$ km s^{-1}. The origin of the systematic redshift of the emission centroid at the several orbital phases is unclear. The effect may be related to the asymmetric nature of the interstellar Lα absorption, especially the extensive damping wings, owing to the 10 km s^{-1} difference between the interstellar and Capella COM radial velocities.

Finally, unlike Mg II *h* and *k*, the Capella Lα features show no clear evidence of "doubling" near elongation. The lack of identifiable contributions from the primary and secondary may be a result of the extreme width of the Lα feature compared with the orbital velocity splitting. In any event, observations with higher signal-to-noise, and taken at the *opposite* elongations, would be useful in establishing the effect of the component Lα profiles on the composite emission envelope.

Figure 4 compares prominent emission features of the Capella short-wavelength spectrum at velocity crossing and near elongation. The phase 52 days profiles are from SWP 1305. The phase 82 days profiles are from SWP 2299, with the exceptions of C IV λ1548 and Si II λ1808, which are saturated in that image. Instead, we used the corresponding C IV and Si II features from SWP 1454, which was taken at phase 81 days of the previous orbit. The profiles in Figure 4 are arranged, from bottom to top, in a sequence of increasing temperature of formation. The center-of-mass velocity scales are as described above. Centroid velocities and FWHMs for the individual features at the two orbital phases are given in Table 4.

Two important conclusions can be drawn from the comparisons in Figure 4 and Table 4. First, at the phase 52 days velocity crossing there is no large systematic velocity shift between the transition region lines (C II, Si IV, C IV, N V) and those formed in the underlying chromosphere (O I, Si II). Our result is contrary to that obtained by Dupree (1976) using *Copernicus*. She found a progression of increasing *blueshifts*, relative to the Lα emission profile, of 15 km s^{-1} for Si III, 25 km s^{-1} for N V, and 32 km s^{-1} for O VI. Dupree interpreted the progression of blue-

shifts as evidence for a massive coronal wind ($\dot{\mathfrak{M}} \approx 10^{-8}\,\mathfrak{M}_\odot\ \mathrm{yr}^{-1}$) emanating from the Capella primary. However, we find in our *IUE* spectra no significant violet displacements of TR lines relative to chromospheric lines. If anything, we find a small *redshift*. (Note: the mean velocity of the TR lines cited in Table 4 is an average of the individual velocities weighted according to the relative line strengths.)

We have confidence in our result because it is based on intercomparisons of many, high–signal-to-noise line profiles on an internally self-consistent velocity scale. In addition, owing to the considerably lower sensitivity of *Copernicus*, Dupree was forced to use the broad Lα emission profile as a chromospheric velocity reference, whereas the extensive data base provided by *IUE* allows us to use the O I and Si II features for that purpose. The latter are narrower than Lα and are formed somewhat deeper in the chromosphere. More importantly, the O I + Si II combination provides at least a crude check on the internal consistency of the *IUE* velocity scale: we have three features to intercompare instead of one, and the O I and Si II lines fall at opposite ends of the *IUE* short-wavelength region. We suspect that at least part of the apparent disagreement between our work and the $\sim 30\ \mathrm{km\ s^{-1}}$ blueshifts of TR lines deduced from the *Copernicus* spectra can be explained by the choice of chromospheric velocity references. In particular, we find that the emission profile of Lα exhibits a $\sim 15\ \mathrm{km\ s^{-1}}$ redshift at velocity crossing relative to the other chromospheric features (see above). In fact, an analogous anomalous behavior of Lα is seen in Dupree's (1976) Figure 3. There, the phase 50 days profiles of Mg II, N V, and O VI all lie within one standard deviation of the system COM radial velocity ($29.5\ \mathrm{km\ s^{-1}}$), consistent with our *IUE* measurements at velocity crossing, while the emission profile of Lα is *redshifted* by about $30\ \mathrm{km\ s^{-1}}$ relative to the COM velocity. We conclude that the $30\ \mathrm{km\ s^{-1}}$ blueshift of O VI deduced by Dupree is not real, but instead is an artifact of the intrinsically asymmetric nature of the Capella Lα profile. Consequently, we find no evidence to support the existence of massive coronal winds from either component of the binary.

Our second and most important conclusion is that virtually all of the transition-region emission, and the bulk of the chromospheric emission, comes from the Capella secondary rather than from the primary. We find that the mean centroid of the high-temperature emission features shifts toward the red from the velocity crossing at phase 52 days to phase 82 days, when the secondary is receding relative to the system center of mass. Furthermore, the low-temperature lines He II, Si II, and O I are all asymmetric near elongation in the same sense as the Mg II resonance lines.

We estimated the fractional contributions of the Capella stars to the composite emission by reflecting the long-wavelength wing of each profile, which presumably is exclusively from the secondary, about the radial velocity of the secondary. Our procedure is illustrated in Figure 5.

In the low-temperature lines, the Capella *primary* provides only about 20–30% of the flux, and in the high-temperature lines the primary accounts for perhaps less than 5%. This is an unexpected result, especially since the primary has nearly 3 times the angular area of the secondary; in terms of *surface flux*, Capella Ab is overwhelmingly brighter than Aa in *all* of the lines. This conclusion is diametrically opposite to previous work which has almost universally assumed that the Capella primary is the major source of the observed UV emission (Dupree 1975, 1976; Haisch and Linsky 1976; Kelch *et al.* 1978; Linsky *et al.* 1978; Doschek *et al.* 1978*b*; but see Katsova and Livshitz 1978).

The assumption that Capella Aa is the predominant UV emitter was based on the observation that the "sharp" Ca II emission features in the composite spectrum follow the radial velocities of the primary rather than the secondary, and the assumption that stars with strong chromospheric Ca II emission are likely to have strong transition-region emission as well. This was certainly a reasonable approach at the time. However, the *IUE* echelle mode data tell us that Capella is a particularly poor case to apply a Ca II–TR emission correlation. The reason is that the contribution of the secondary to the total Ca II emission cannot be judged reliably because the Capella Ab Ca II emission cores appear to be diffuse or "washed out" compared with those of Capella Aa (see Baliunas *et al.* 1979). The problem is less severe for the Mg II lines because the *h* and *k* features typically exhibit much greater core-wing contrasts than the Ca II features. The apparent contrast is enough that the secondary contribution to the composite Mg II profile is readily identifiable near elongation. In fact, using the profile reflection procedure, we estimate that only about a third of the Mg II flux at phase 82 days is from the primary.

This result is rather important. Our previous study (Paper III) of the solar-like binary α Centauri revealed that both components have similar surface fluxes in the Ca II and Mg II lines, and also in the hotter emission lines of the 1150–2000 Å region. We concluded that the two rather similar dwarf stars in the widely separated ($P = 80$ yr) α Centauri system have very similar—and quiet—chromospheres and transition regions. On the other hand, we find in the Capella system two giant stars, which are ostensibly even more similar to each other than α Cen A is to α Cen B, but which have extraordinarily different levels of chromosphere-corona activity. To stress this point, we have estimated component *surface* fluxes for the strongest lines of Table 3, assuming that the contribution of the primary to the observed emission is 1/3 for Mg II and decreases with increasing temperature of formation to 1/20 for the transition-region lines. (The latter estimate is of course very uncertain.) The derived Aa and Ab surface fluxes are compared in Table 5 with the corresponding quiet-Sun surface fluxes. The solar

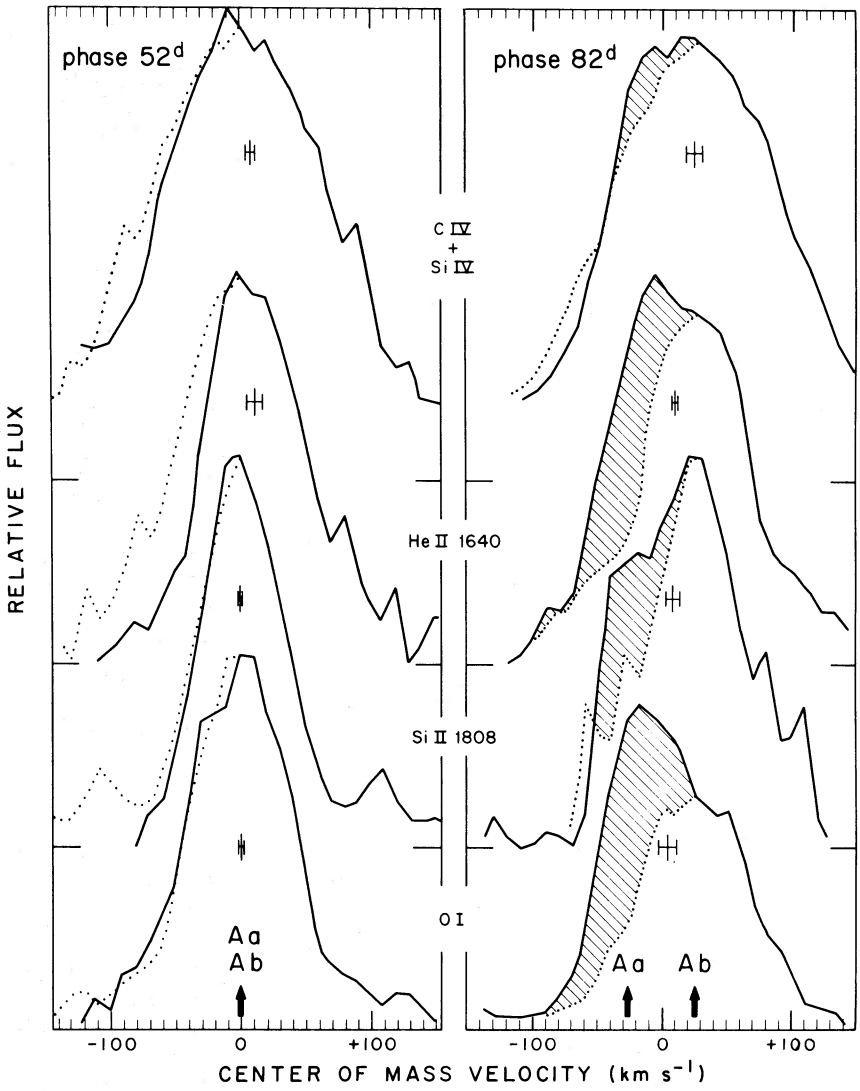

FIG. 5.—Summary of high-resolution profiles at velocity crossing and near elongation. The C IV + Si IV and O I line shapes are composites of several individual features combined on a common velocity scale to improve the signal-to-noise ratio of systematic velocity patterns. Line bisectors (Table 5) are indicated at the two orbital phases. The dotted curves are the long-wavelength wings of each profile reflected about the Capella *secondary's* radial velocity. At velocity crossing the profiles are symmetric about $V_{Ab} = V_{COM} = 0$ (with the exception of the He II + Fe II λ1640 blend). Near elongation, the low-temperature features O I and Si II become asymmetric, but the high-temperature C IV–S IV composite profile remains relatively symmetric about the Ab velocity. The shaded portions of the elongation profiles represent the estimated contribution of the Capella *primary* to the individual line shapes, according to the profile reflection procedure.

values were determined from the degraded solar spectrum illustrated in Figure 1 using the same techniques as were applied to the *IUE* low-dispersion spectra of Capella, so as to minimize possible systematic effects in the solar-stellar comparison (see Paper III). It is clear from Table 5 that the Capella primary has surface fluxes in all lines which are similar to quiet solar values, whereas the secondary has surface fluxes a factor of 50 larger. The Capella primary therefore has a more nearly solar-like outer atmosphere, while that of the secondary is considerably different. The previous models constructed for Capella must be reevaluated in this light.

IV. DISCUSSION

a) Is Rotation the Key?

Any discussion of the Capella system must first address the question of why these ostensibly similar giant stars exhibit very different levels of chromosphere-corona emission. We propose that the dichotomy arises from the only property that is obviously different in the two stars, namely rotation; the primary has a sharp-line spectrum and presumably is a slow rotator like most G and K giants ($V \sin i \lesssim 5$ km s^{-1}; e.g., Smith and Dominy 1979), whereas the secondary has a diffuse spectrum (Struve and Kung 1953; Wright

TABLE 5

SURFACE FLUXES AND FLUX RATIOS

Approximate Wavelength (Å)	Line	$\mathscr{F}_l^{\odot}(10^3)$[a,d]	$f_l^*(10^{-11})$[a]	Assumed (f_l^{Aa}/f_l^*)	$\mathscr{F}_l^{Aa}(10^3)$[a]	$\mathscr{F}_l^{Aa}/\mathscr{F}_l^{\odot}$	$\mathscr{F}_l^{Ab}(10^3)$[a]	$\mathscr{F}_l^{Ab}/\mathscr{F}_l^{\odot}$
(0.15–2.8 keV)	(soft X-rays)	16[e]	17[f]	0.05	22	1.4	1100	70
1032	O VI	1.0[g]	0.9[h]	0.05	1.1	1.1	58	60
1175	C III	1.6	1.8[c]	0.05	2.3	1.4	120	80
1216	Lα + Si III	230	31[b]	0.33	260	1.1	1400	6
1240	N V	0.9	1.3[c]	0.05	1.7	2	84	90
1305	O I	4.0	4.9[c]	0.25	31	8	250	60
1335	C II	4.6	2.7[c]	0.05	3.4	0.7	180	40
1400	Si IV	2.5	2.3[c]	0.05	2.9	1.2	150	60
1550	C IV	5.8	4.4[c]	0.05	5.6	1.0	280	50
1640	He II + Fe II	1.3	0.7[c]	0.25	4.6	4	37	30
1660	C I	5.3	1.2[d]	0.33	10	1.9	54	10
1815	Si II	16	5.1[c]	0.25	33	2	260	16
2796	Mg II *k*	600	70	0.33	600	1.0	3200	5
3934	Ca II K	420	86[i]	0.33	730	1.7	3900	9

[a] $\mathscr{F}$ = surface flux = ergs cm^{-2} s^{-1} at star; f = apparent flux = ergs cm^{-2} s^{-1} at Earth.

[b] No correction for interstellar absorption or geocoronal emission.

[c] Includes all members of multiplet.

[d] Ayres and Linsky 1980, unless otherwise indicated.

[e] $L_x^{\odot} \approx 1 \times 10^{27}$ ergs s^{-1} (Topka *et al.* 1979).

[f] $L_x^* \approx 4 \times 10^{30}$ ergs s^{-1} (Cash *et al.* 1978).

[g] $\mathscr{F}_l^{\odot} \approx \pi I_l^{\odot}$, $I_l^{\odot}$ is quiet-Sun average (Vernazza and Reeves 1978).

[h] $f_l^* = 0.47$ photons cm^{-2} s^{-1} at Earth (Dupree 1975).

[i] Kelch *et al.* 1978.

1954; Franklin 1959; Wallerstein 1966; Boesgaard 1971) and presumably is a rapid rotator. Herbig and Spalding (1955) estimated $V \sin i \approx 85$ km s^{-1} for the Capella secondary based on the similarity between what they decided was the Ab spectrum and that of the rapid rotator 31 Comae. Theirs must be a large overestimate since the measured FWHM of Si II λ1808 is only 64 km s^{-1}, and that feature is probably broadened by nonthermal motions and significant optical depth as well as rotation. Struve and Kung (1953) and Franklin (1959) have remarked that the photospheric absorption spectrum of the Capella secondary is qualitatively similar to that of the F5 supergiant α Per, although the Ab lines are somewhat broader. Uesugi and Fukuda (1970) and Herbig and Spalding (1955) have assigned $V \sin i \approx 20$ km s^{-1} to α Per. Finally, Boesgaard (1971) has commented that weak lines in the secondary spectrum of Capella are difficult to measure owing to a rotational broadening of 10–12 km s^{-1} (see also Franklin 1959). However, visual inspection of the Ab Li I λ6708 absorption feature (FWHM ≈ 60 km s^{-1}) in her tracings suggests a significantly larger $V \sin i$.

In order to provide a better estimate of the secondary's rotation, we compared simple rotational profiles to the Li I λ6708 line. Our results are depicted in Figure 6. The empirical line shape is a symmetrized profile based on the two tracings illustrated in Boesgaard's Figure 2. The synthetic rotational profiles are for an intrinsically narrow feature of constant center-to-limb behavior, and for a continuum limb-darkening coefficient, $\epsilon = 0.5$ (see Gray 1976). Our results are not overly sensitive to the latter parameter. We conclude that the projected rotational velocity, $V \sin i$, of the Capella secondary is $\lesssim 30$ km s^{-1}. (The latter corresponds to an equatorial rotational velocity of $V \approx 40$ km s^{-1} if the stellar rotation is in the plane of the primary orbit.) In short,

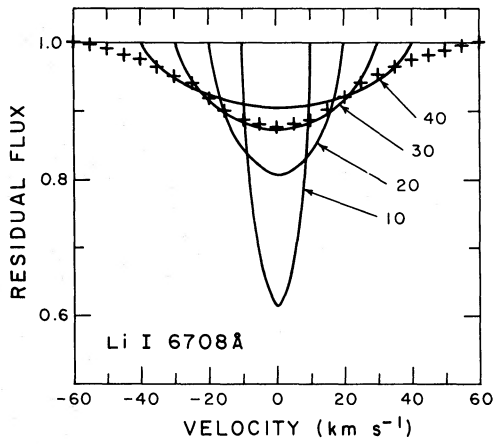

FIG. 6.—Comparison of simple rotational profiles (*solid curves*) with the Capella Ab Li I λ6708 absorption features (*pluses*). The individual rotational profiles have been normalized to the same equivalent width. A value of $V \sin i$ near 30 km s^{-1} is indicated by the comparison.

the $V \sin i$ of the Capella secondary is very likely considerably larger than that of the primary.

The rotation dichotomy between the Capella primary and secondary is plausible in light of the evolutionary scenario proposed for the system (see § II*b*). In particular, the primary has probably spent a considerably longer time as a late-type star, with a convective envelope and a chromosphere-corona, than the less massive and more slowly evolving secondary. Consequently, the Capella primary has probably had ample opportunity to lose the rapid rotation of its main-sequence progenitor, a late-B or early-A dwarf, through magnetic braking (see Kraft 1967 and references therein), or perhaps by mass loss prior to and at helium flash (Iben 1965). The secondary, on the other hand, has only recently begun its post–main-sequence evolution, and may not yet have had adequate time to shed much of its rotational velocity by magnetic braking or evolutionary expansion.

The Capella secondary therefore shares important properties with short-period RS CVn-type binary systems (cf. Hall 1978): large ultraviolet surface fluxes, intense soft X-ray emission (assuming that Ab is indeed responsible for the bulk of the detected coronal X-rays), and rapid rotation. In the case of the Capella secondary, rapid rotation is an accident of youth. In the case of the short-period RS CVn-type binaries, high rotation rates are enforced by tidal coupling and, therefore, are an accident of environment (Hall 1978).

We expect that the enhanced chromosphere-corona activity of a rapidly rotating star such as the Capella secondary, compared with similar but slowly rotating giants like the primary, is a result of a stronger hydromagnetic dynamo. Parker (1970) has shown that the strength of the dynamo is governed by the interaction between convective motions and rotation-driven coriolis forces. Since the dynamo is thought to be the source of stellar surface magnetic fields and the activity associated with them (cf. Vaiana and Rosner 1978), one would expect a brighter chromosphere-corona in convective stars that are rapid rotators. The idea of a rotation-activity connection is by no means novel. Such a correlation was recognized over a decade ago in chromospheric Ca II emission strengths (Wilson 1966; Kraft 1967; Skumanich 1972).

Not surprisingly, a rotation-activity correlation is also seen in coronal soft X-ray sources. For example, the brightest *coronal* sources detected in the low-energy *HEAO 1* all-sky survey are typically RS CVn-type binaries (Walter, Charles, and Bowyer 1978). Such systems exhibit X-ray–to–bolometric luminosity ratios, L_x/L_{bol}, of order 10^{-3}. The stars in these short-period, but detached, systems are rapid synchronous rotators by virtue of tidal friction. Typical equatorial rotation rates are of order 40 km s^{-1} for the K subgiant secondaries (which have larger radii than the F-G dwarf primaries, and consequently rotate faster in a synchronous situation). On the other hand, isolated G-K dwarf stars such as the Sun, or slowly rotating

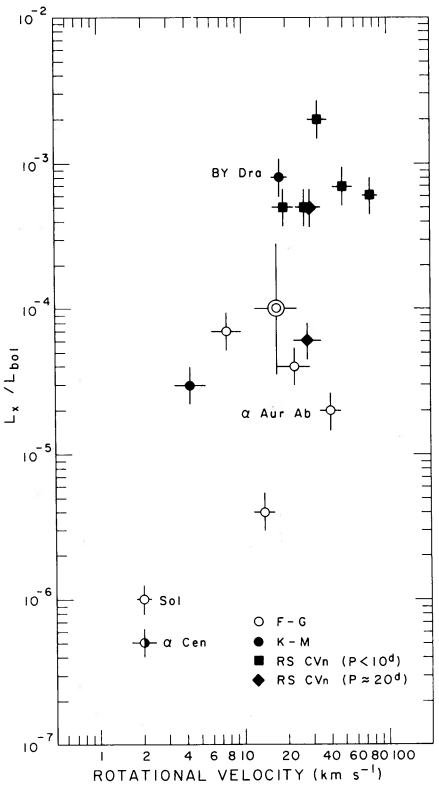

FIG. 7.—The proposed rotation-activity connection among coronal soft X-ray sources. The quantity L_x/L_{bol} is the fraction of the stellar luminosity that is emitted in the 0.15–3 keV soft X-ray region. The double concentric circle represents the average of five 2 σ detections of F6–F7 dwarfs from the *HEAO 1* all-sky survey. The sources are subdivided into hot (F-G) and cool (K-M) late-type stars, and RS CVn-type binary systems (which typically contain a K-type subgiant secondary that is the more "active" of the two components). Note that the fast rotators tend to have large L_x/L_{bol} ratios, while the slowly rotating, solar-type dwarfs (the Sun, α Cen A and B) have small L_x/L_{bol} ratios. Note also that at a given rotational velocity, the stars of later spectral type tend to have larger L_x/L_{bol} ratios than the earlier-type stars.

dwarf components of well-separated binaries, α Centauri A and B for example, typically exhibit L_x/L_{bol} ratios of order 10^{-6} or less (Nugent and Garmire 1978; Topka *et al.* 1979). The equatorial rotation velocities of these stars are a few km s^{-1} or less (Smith 1980). In addition, slowly rotating K giants such as Arcturus (α Boo, K2 III) and Aldebaran (α Tau, K5 III) were not detected in the *HEAO 1* survey at L_x/L_{bol} levels comparable to the mean Sun or α Centauri.

Figure 7 and Table 6 summarize the rotation-activity connection in coronal soft X-ray sources.

We established L_x/L_{bol} ratios using published soft X-ray fluxes (0.15–3 keV), visual magnitudes from the Bright Star Catalog (Hoffliet 1964), and bolometric corrections appropriate to the stellar spectral types (Allen 1973). We determined equatorial rotational velocities V for the short-period ($P \lesssim 20$ days) RS CVn-type systems assuming synchronous rotation.

TABLE 6

THE ROTATION-ACTIVITY CONNECTION IN CORONAL SOFT X-RAY SOURCES

Star	Spectral Type	$L_x/L_{bol}(10^{-4})$	V (km s^{-1})
Sun	G2 V	0.01[a]	2[d]
χ^1 Ori	G0 V	0.7[a]	(6)[e,f]
η Boo	G0 IV + ?	0.04[a]	14[f]
α Cen	G2 V + K1 V	0.005[a]	2[g]
70 Oph	K0 V + K5 V	0.3[a]	(3.3)[e,h]
5 2$^\sigma$ sources	F6 V–F7 V	1 ± 0.45 dex[a]	(13 ± 4)[e,f]
LX Per	G5 IV + G5 IV	5[b]	22, 16[i]
UX Ari	G5 V + K0 IV	5[b]	23, 31[i]
HR 1099	G5 V + K0 IV	7[b]	42, 57[i]
RS CVn	F4 IV–V + K0 IV	20[b]	28, 38[i]
AR Lac	G2 IV + K0 IV	6[b]	76, . . .[i]
HK Lac	K0 III + ?	5[b]	29, . . .[i]
σ Gem	K1 III + ?	0.6[b]	(22), . . .[e,f]
α Aur Ab	F9 III	0.2[b]	40[j]
μ Dra	dF6 + dF6	0.4[c]	(23, 13)[e,f]
BY Dra	dM0e	8[c]	18[k]

[a] Walter, *et al.* 1980.

[b] Walter *et al.* 1978.

[c] Ayres *et al.* 1979.

[d] Allen 1973.

[e] Parentheses indicate $V \sin i$ rather than V itself.

[f] Uesugi and Fukuda 1970.

[g] Boesgaard and Hagen 1974.

[h] Smith 1980.

[i] Synchronous rotation.

[j] This work for $V \sin i = 30$.

[k] Vogt and Fekel 1979.

For the remaining stars, we obtained $V \sin i$ from published work, primarily the catalog of Uesugi and Fukuda (1970). We included only *firm* measurements of $V \sin i$; upper limits were not considered. If the orbital inclination was available, we converted $V \sin i$ to V, assuming that the rotational and orbital axes are similar. In the remaining cases, we multiplied the measured $V \sin i$ (given in parentheses in Table 6), by the inverse mean projection factor, $\langle \sin i \rangle^{-1} = 4/\pi$, to minimize systematic effects introduced by the unknown stellar inclinations.

The double open circle in Figure 7 represents an average of five marginal (2σ) detections from the *HEAO 1* all-sky survey (Walter *et al.* 1980). The five source candidates are F6 or F7 dwarfs with rotational velocities listed in the catalog of Uesugi and Fukuda. The vertical extent of the plotted cross indicates the dispersion among the individual L_x/L_{bol} ratios of the 2σ detections.

We have provided Figure 7 here solely to illustrate that the brightest coronal sources tend to be fast rotators. Considerable uncertainties are inherent in constructing such a diagram, and it must be considered preliminary. For example, the sensitivity and temporal coverage of the available soft X-ray detections (primarily from *HEAO 1*) are limited; high-quality rotational velocity measurements of cool stars (e.g., Smith 1980) are comparatively few; and the sample of coronal sources is not uniform. These uncertainties and selection effects dictate that any effort to draw additional conclusions from Figure 7, beyond the existence of the rotation-activity correlation itself, is premature. A concerted effort to obtain extensive, uniform, and systematic soft X-ray measurements of cool stars, as well as high-quality spectroscopic determinations of projected rotational velocities, is clearly warranted.

In any event, rotation is only part of the coronal activity story. Other stellar properties—convection zone depth, for example—must play equally important roles. For example, the Capella secondary has an equatorial rotation velocity comparable to the RS CVn-type secondaries, but an L_x/L_{bol} ratio only 5% as large. Here, the more extensive convection zones of the cooler RS CVn-type secondaries perhaps enhance dynamo action, compared with the thin surface convective zones in F-type stars such as the Capella secondary. Some support for the importance of convection zone depth is provided by the BY-Draconis–type dMe flare stars. Several of these were detected by *HEAO 1* as quiescent X-ray emitters at L_x/L_{bol} levels comparable to the RS CVn systems (Ayres *et al.* 1979). The BY-Dra flare stars tend to be rapid rotators compared with similar, but nonactive, stars on the lower main sequence (Bopp and Fekel 1977). In fact, Bopp and Fekel propose that rotation,

rather than duplicity, is the essential ingredient in the BY-Draconis "syndrome." However, the inferred equatorial rotation rate for BY Dra, in particular, is smaller than those of the synchronously rotating RS CVn's despite the similar L_x/L_{bol} levels (Table 6). On the other hand, the dMe flare stars are thought to have fully convective interiors, unlike G-K dwarfs and giants, which have shallow convective envelopes.

If rotation is a fundamental ingredient in the chromosphere-corona activity of cool stars, then the outer atmosphere is in a sense a self-defeating phenomenon. The magnetic braking of the surface layers is probably positively correlated with the mean activity level, which in turn depends on the rotation rate. Consequently, the more active the chromosphere-corona, the faster the spindown rate and the faster the chromosphere-corona becomes weaker. However, short-period binary systems should not suffer the rapid spindown of isolated stars owing to the large reservoir of orbital angular momentum available to maintain synchronous rotation through tidal coupling.

b) The Work of Katsova and Livshitz

Katsova and Livshitz (1978) have previously suggested that the Capella secondary rather than the primary is the principal UV emission source. Their argument is based on theoretical calculations (e.g., de Loore 1970) which predict that late-F giants should have brighter chromospheres than middle-G giants owing to enhanced *acoustic flux* production in the hotter convective stars. Katsova and Livshitz proposed a colliding stellar wind model to reconcile the measured UV and soft X-ray emission with the blueshifts found by Dupree (1976). However, their dynamical model is inconsistent with our data, which imply no large-scale systematic gas flows. In addition, it is hard to see how the relatively modest difference in spectral type between the Capella primary and secondary alone could be responsible for the factor of 50 difference in UV surface fluxes. Finally, the detected soft X-ray emission from Capella is entirely consistent with a solar-like (albeit very active) corona; hence the intrastellar shock emission mechanism proposed by Katsova and Livshitz is not necessary to reconcile coronal and transition-region properties.

c) Comments on Previous Outer Atmosphere Models of Capella

Several chromospheric and transition-region models have been proposed for Capella based on Ca II and Mg II fluxes (Kelch *et al.* 1978; Baliunas *et al.* 1979) and UV line intensities (Haisch and Linsky 1976; Doschek *et al.* 1978*b*). One of the important parameters that ties together models of the chromosphere, transition region, and corona is the coronal base pressure P_0. Different TR structures seen on the Sun (coronal holes, quiet Sun, active regions, and flares) all appear to have a geometrical thickness smaller than the local pressure scale height. The gas pressure should therefore be constant in the TR, if the TR is in hydrostatic equilibrium, and the TR pressure should equal the pressure at the top of the chromosphere and at the base of the corona. The upper chromosphere pressure can be estimated from the emission core strengths of Lα, Mg II *h* and *k*, and, to a lesser extent, Ca II H and K (cf. Basri *et al.* 1979; Ayres and Linsky 1976). The TR pressure itself can be determined directly using density-sensitive line ratios (Doschek *et al.* 1978*b*), or indirectly from the emission measures of collisionally excited resonance lines (Haisch and Linsky 1976). Finally, the coronal base pressure can be estimated from coronal emission measures and temperatures deduced from soft X-ray observations.

In previous work, conflicting results have been obtained for coronal base pressures derived using Ca II and Mg II line strengths, TR line ratios, and TR line strengths. The sense of the disagreement is 0.1:1:10, respectively, where unity is the quiet-Sun pressure $P_0^{\odot} \approx 0.3$ dynes cm^{-2} (Doschek *et al.* 1978*a*). These estimates were all obtained on the assumption that the Capella primary is the major source of line emission. However, an important result of our work is that the secondary is the dominant emitter. How does this recognition change the previous pressure estimates?

First, the chromospheric models based on the Ca II and Mg II lines were constructed for the "wrong" star, at least in terms of comparing coronal base pressures. It is therefore not surprising that the derived pressures for the top of the chromosphere disagree significantly with the pressures estimated by Haisch and Linsky (1976) for Capella's transition region. If we were to redo the Capella chromosphere models of Kelch *et al.* (1978), we would have to take into account the somewhat different stellar parameters of Capella Ab compared with Aa, and the significantly enhanced surface fluxes of Ca II and Mg II in the secondary. Since the Capella primary and secondary are very similar types of stars, we expect the second effect to be more important. For example, we estimate an Mg II $h + k$ surface flux of 6×10^6 ergs cm^{-2} s^{-1} for the Capella secondary. This is very nearly the surface flux predicted by the Kelch *et al.* (1978) model *C* ($\mathcal{F}_{\rm Mg\,II} \approx 5 \times 10^6$ ergs cm^{-2} s^{-1}), which has a mass column density of $m_0 = 1 \times 10^{-4}$ g cm^{-2} at the top of the chromosphere and, therefore, for the base of the corona. Given the relatively weak dependence of $\mathcal{F}_{\rm Mg\,II}$ on m_0 seen for example in solar models ($\mathcal{F}_{\rm Mg\,II} \sim m_0^{1/3}$; Ayres and Linsky 1976), we estimate that $m_0 \approx 2 \times 10^{-4}$ would reproduce the observed Ab Mg II flux. Since the surface gravity of the Capella secondary is roughly 1.4×10^3 cm s^{-2}, the upper chromosphere pressure is $P_0 \approx g m_0 \simeq 0.3$ dynes cm^{-2}, which is comparable to the solar value.

Second, TR density estimates derived from line ratios will not change, but the star to which they refer is now the secondary. The Doschek *et al.* (1978*b*) study was based on the early Capella ob-

TABLE 7

DENSITY DIAGNOSTIC LINE RATIOS

	Si IV λ1403	O III λ1666	Si III λ1892	C III λ1909
$\mathscr{F}_l^{Ab}$ (10^4 ergs cm^{-2} s^{-1}).....	5	2.1	17	5
		Flux Ratio	P_0[a] (dynes cm^{-2})	
O III/*Si* IV.....		0.42	0.4	
C III/*Si* IV.....		1.0	0.5	
C III/*O* III.....		2.4	0.4	
C III/*Si* III.....		0.3	0.3	

[a] $P_0 \approx 2n_e kT$; $T \approx 6 \times 10^4$ K; $P_0^{\odot} \approx 0.3$ (Doschek *et al.* 1978*a*).

servations obtained during the scientific commissioning phase of *IUE*. Only a crude flux calibration was available for those data. We have therefore rederived the C III λ1909/Si III λ1892 flux ratio using the accurately calibrated low-dispersion composite spectrum (§ II*b*[i]) as a transfer standard to place the high-dispersion Si III and C III profiles on an absolute flux scale. We have also measured emission strengths of O III λ1666 and Si IV λ1403 to compare with additional density diagnostic ratios calculated by Doschek *et al.* (1978*a*). The results of that comparison are summarized in Table 7. The fluxes of the O III, Si III, and C III features are uncertain by perhaps ±20% owing to the poorly defined continuum levels. As a result, we expect factors of at least 2 uncertainties in the derived densities. In applying the theoretical density diagnostic ratios to the measured ratios we have used the *unscaled* relations given by Doschek *et al.* (1978*a*), instead of the "scaled theoretical" curves. The latter were empirically adjusted to account for the relative sensitivity of the NRL normal-incidence spectrograph on *Skylab* and are not relevant to the low-dispersion mode of *IUE*, which has an absolute flux calibration. The pressures estimated from the four line ratio combinations are similar to each other and are consistent with the previous work by Doschek *et al.* (1978*b*). The most sensitive of the diagnostics in this particular density regime is C III/Si IV. The measured ratio implies a pressure of $P_0 \approx 0.5$ dynes cm^{-2} at a mean temperature of formation of 6×10^4 K. The other ratios suggest comparable or somewhat smaller pressures. All are consistent with $P_0^{Ab} \approx P_0^{\odot}$ to within a factor of 2.

The consistency of the C III/Si III pressure estimate with the other density diagnostic ratios suggests the upper chromosphere of the Capella secondary may not have a temperature plateau near $T = 2 \times 10^4$ K, which would preferentially strengthen the Si III λ1892 feature. Such a plateau has been proposed for the quiet Sun (Tripp, Athay, and Peterson 1978) and the K dwarf ε Eri (Simon, Kelch, and Linsky 1979), but is apparently absent in strong plages (Basri *et al.* 1979). In fact, the TR pressures for the Capella secondary, based on density-sensitive line ratios, are comparable to the TR pressures estimated in the cooler, more active stars in RS CVn systems. For example, Simon and Linsky (1980) have derived TR pressures of 0.2–0.6 dynes cm^{-2} in HR 1099 and UX Ari, while Simon, Linsky, and Schiffer (1980) have proposed that the TR pressure in the UX Ari secondary increased to 1.1 dynes cm^{-2} during a large flare.

Despite the consistency we find among the several density diagnostic line ratios, we caution that the C III/Si III ratio, in particular, may be subject to systematic errors owing to the neglect of charge-transfer processes in the original ionization equilibrium calculations (see Baliunas and Butler 1980). Nevertheless, the C III/Si III ratio we derive for the Capella secondary is similar to that quoted for the quiet Sun (Doschek *et al.* 1979*b*). Consequently we expect that the TR pressures in the Capella secondary are similar to those of the quiet Sun, even though the *absolute* pressure we have obtained from the C III/Si III ratio may be in error.

Finally, we consider pressure estimates based on emission line strengths (or, equivalently, emission measures) and the assumption of a thermal-conduction–dominated TR. If the divergence of the conductive flux within the TR is balanced locally by radiative losses and the abundances are solar, then surface fluxes of collisionally excited resonance lines, such as the Si IV, C IV, and N V doublets, should scale from solar values directly as the ratio of coronal base pressures (Haisch and Linsky 1976). For example, Haisch and Linsky proposed that P_0 for the Capella primary should be roughly 10 times solar, since surface fluxes of the then available ultraviolet line observations were essentially 10 times solar, assuming that the Capella primary was in fact the emission source. We now know that the Capella secondary is the dominant emitter and that the mean surface flux enhancement of TR lines in the giant is 50 times the quiet Sun. Therefore, the conduction-dominated model would predict a P_0 of 50 times solar ≈ 15 dynes cm^{-2}.

Recently, Baliunas *et al.* (1979) have attempted to reconcile the low coronal base pressure implied by the Kelch *et al.* (1978) Capella Aa chromosphere model

with the high-pressure TR proposed by Haisch and Linsky. Baliunas *et al.* demonstrate that the low-pressure chromosphere derived by Kelch *et al.* is by no means unique, and they propose a chromospheric thermal structure that is compatible with the observed Ca II and Mg II emission and the Haisch and Linsky TR pressure. However, Baliunas *et al.* assumed that the Capella primary is the dominant UV emitter, and it is not clear whether their rather extreme class of chromospheric models can explain the very large TR pressure which would be implied by a Haisch-Linsky–type analysis of the Capella secondary's surface fluxes. Furthermore, Baliunas *et al.* cite pressures estimated from the C III $\lambda\lambda$1176/977 density diagnostic as support for the high-pressure Capella models. However, the observed C III ratio implies $P_0 \approx 1$ dynes cm^{-2}, which is much more compatible with the intermediate values of P_0 based on other density diagnostics (Table 7), than with the order-of-magnitude larger P_0 that would be inferred from a Haisch-Linsky–type interpretation of the Ab TR emission.

To summarize, we find that coronal base pressures estimated for the Capella secondary by several independent methods are consistent with the quiet-Sun base pressure, but that derived on the assumption of a conduction-dominated energy balance is more than an order of magnitude larger than the other estimates. We conclude that transition-region pressures of the Capella secondary are of order 0.5 dynes cm^{-2}. Consequently, the transition region of the Capella secondary is unlikely to be heated significantly by electron conduction from the overlying corona.

d) Is Capella Ab Like a Sunspot?

If coronal base pressures in the Capella secondary are essentially solar, then that star shares important properties in common with sunspots. Foukal *et al.* (1974), Noyes (1974), and Foukal (1975) have described the intense emission in 10^5 K lines that is commonly seen in plumelike structures near sunspot umbrae in *Skylab* spectrophotometry (see also Cheng, Doschek, and Feldman 1976). The sunspot plume emission in moderate-temperature lines (e.g., Lα) is comparable to that of the surrounding plage (Basri *et al.* 1979), and is roughly a factor of 5 brighter than the quiet Sun. However, the plume emission in lines of O IV (10^5 K), O VI (3×10^5 K), and Ne VII (7×10^5 K) can be 10 times that of the surrounding plage and up to 100 times that of the quiet Sun (Foukal *et al.* 1974, their Fig. 3). Moreover, these enormous emission enhancements are not accompanied by the correspondingly large pressures that would be predicted by conduction-dominated TR models. Instead, the inferred pressures are less than those of typical plages (Foukal 1975) and in fact may be comparable to quiet-Sun pressures (Noyes 1974). The simplest way of explaining enhanced emission in 10^5 K lines at low pressures is to flatten the TR temperature gradient. This increases the thickness of the TR over a given temperature range, and hence also the amount of material that can radiate at those temperatures (Noyes 1974). However, reducing the temperature gradient is tantamount to reducing the importance of heat conduction in the local energy balance, since the conductive flux carried through any layer of the atmosphere is proportional to dT/dh.

Thus the Capella secondary exhibits the ultraviolet spectral properties of the cool plumes of plasma commonly seen near sunspot umbrae. What is a relatively isolated, small-scale phenomenon on the Sun may be a much larger-scale phenomenon on the Capella secondary, and perhaps also in the even more active RS CVn-type systems which are well known to exhibit the photometric symptons of "spottedness" (Hall 1978).

e) Why Are the 10^5 K Lines So Broad?

The profiles of high-temperature lines in the Capella Ab spectrum are very broad ($\langle \mathrm{FWHM} \rangle \gtrsim 100$ km s^{-1}), suggesting possible mass motions greatly exceeding the local sound speed at 10^5 K. Is it possible to reconcile the large line widths with a subsonic atmosphere?

There are at least two mechanisms that can produce the large line widths without recourse to hypersonic nonthermal broadening.

The first mechanism is "opacity broadening." We might expect resonance lines such as Si IV, C IV, and N V to be at least 50 times more opaque in the Capella secondary than in the quiet Sun. In a slab geometry, enhanced opacity can produce broader lines for the same intrinsic Doppler width. However, to produce the entire widths of the Capella Ab features, which are typically 3 times broader than the corresponding solar TR lines (White and Lemaire 1976), with solar nonthermal velocities would require line-center optical depths (τ_{lc}) of greater than 10^4. Since the Si IV, C IV, and N V doublets are probably optically thin in the quiet Sun (Roussel-Dupre, Francis, and Billings 1979), we would expect $\tau_{lc} \lesssim 50$ in Capella for these features. Even though opacity broadening is unlikely to account for the entire widths of the TR lines in Capella, it may be responsible for part of the broadening in the most opaque lines and perhaps explains why the C IV features are somewhat broader than the less opaque N V features (Table 5).

A second broadening mechanism is rotation. Rotation would be particularly effective if the EUV emitting structures are coronal loops that extend significantly above the stellar surface, if the loops corotate with the photospheric plasma, and if the activity centers are equatorially concentrated, as they are in the Sun.

f) Concluding Remarks

It is clear that we are groping to understand the structure and energy balance of cool-star transition regions and coronae. We now have the luxury of significantly improved stellar observations, which can

tell us, for example, that the Capella secondary is the key to understanding the unusual properties of the Capella spectrum, but the stellar observations still lack the important quality of spatial resolution. We feel that the answers to many of the questions concerning stellar chromospheres and coronae must be searched for on the Sun. Only on the Sun are we ever likely to have sufficient spatial resolution to probe the morphology and dynamics of small-scale surface features, which may in turn be more nearly global phenomena on other stars. Stellar observations must complement the solar work, because the Sun confronts us with one unchanging set of fundamental stellar parameters. We must therefore look to stars to try to understand how solar structural features may be modified by very different underlying physical conditions. In short, stellar observations can provide a gross overview of chromosphere-corona properties in late-type stars, but the Sun ultimately must provide the details.

This work is supported in part by NASA under grants NAS5-23274 and NGL-06-003-057 to the University of Colorado. We wish to thank Dr. A. Boggess and the staff of the *IUE* observatory for their assistance in the acquisition and reduction of these data. We also thank Dr. K. B. Gebbie for her critical reading of the manuscript.

REFERENCES

Allen, C. W. 1973, *Astrophysical Quantities* (3d ed; London: Athlone).
Ayres, T. R., and Linsky, J. L. 1976, *Ap. J.*, **205**, 874.
———. 1980, *Ap. J.*, **235**, 76 (Paper III).
Ayres, T. R., Linsky, J. L., Garmire, G., and Cordova, F. 1979, Ap. J. (Letters), **232**, L117.
Ayres, T. R., Marstad, N., and Linsky, J. L. 1980, preprint.
Baliunas, S. L., Avrett, E. H., Hartmann, L. W., and Dupree, A. K. 1979, *Ap. J. (Letters)*, **233**, L129.
Baliunas, S. L., and Butler, S. E. 1980, *Ap. J. (Letters)*, **235**, L45.
Barry, D. C., Cromwell, R. H., and Schoolman, S. A. 1978, *Ap. J.*, **222**, 1032.
Basri, G. S., and Linsky, J. L. 1979, *Ap. J.*, **234**, 1023.
Basri, C. S., Linsky, J. L., Bartoe, J.-D. F., Brueckner, C. E., and Van Hoosier, M. E. 1979, *Ap. J.*, **230**, 924.
Batten, A. H., Fletcher, J. M., and Mann, P. J. 1978, *Pub. Dom. Ap. Obs.*, **15**, 121.
Blazit, A., Bonneau, D., Josse, M., Koechlin, L., Labeyrie, A., and Onéto, J. L. 1977, *Ap. J. (Letters)*, **217**, L55.
Boesgaard, A. M. 1971, *Ap. J.*, **167**, 511.
Boesgaard, A. M., and Hagen, W. 1974, *Ap. J.*, **189**, 85.
Boggess, A., *et al.* 1978, *Nature*, **275**, 372.
Bohlin, R. C., Holm, A. V., Savage, B. D., Snijders, M. A. J., and Sparks, W. M. 1979, preprint.
Böhm-Vitense, E. 1980, preprint.
Bopp, B. W., and Fekel, F., Jr. 1977, *A.J.*, **82**, 490.
Cash, W., Bowyer, S., Charles, P., Lampton, M., Garmire, G., and Riegler, G. 1798, *Ap. J. (Letters)*, **223**, L21.
Cheng, C. C., Doschek, G. A., and Feldman, U. 1976, *Ap. J.*, **210**, 836.
Code, A. D., and Meade, M. R. 1979, *Ap. J. Suppl.*, **39**, 195.
Cohen, L., Feldman, U., and Doschek, G. A. 1978, *Ap. J. Suppl.*, **37**, 393.
de Loore, C. 1970, *Astr. Space Sci.*, **6**, 60.
Doschek, G. A., Feldman, U., Bhatia, A. K., and Mason, H. E. 1978*a*, *Ap. J.*, **226**, 1129.
Doschek, G. A., Feldman, U., Mariska, J. T., and Linsky, J. L. 1978*b*, *Ap. J. (Letters)*, **226**, L35.
Dupree, A. K. 1975, *Ap. J. (Letters)*, **200**, L27.
———. 1976, in *Physique des mouvements dans les atmospheres stellaires*, ed. Cayrel and Steinberg (Paris: CNRS), p. 439.
Dupree, A. K., Baliunas, S. L., and Shipman, H. 1977, *Ap. J.*, **218**, 361.
Finsen, W. 1975, *IAU Comm. 26 Circ. d'Inf.*, No. 66.
Flannery, B. P., and Ayres, T. R. 1978, *Ap. J.*, **221**, 175.
Foukal, P. V. 1975, *Solar Phys.*, **43**, 327.
Foukal, P. V., Huber, M. C. E., Noyes, R. W., Reeves, E. M., Schmahl, E. J., Timothy, J. G., Vernazza, J. E., and Withbroe, G. L. 1974, *Ap. J. (Letters)*, **193**, L143.
Franklin, K. L. 1959, *Ap. J.*, **130**, 139.
Gray, D. F. 1976, *The Observation and Analysis of Stellar Photospheres* (New York: Wiley-Interscience), chap. 17.
Haisch, B. M., and Linsky, J. L. 1976, *Ap. J. (Letters)*, **205**, L39.
Haisch, B. M., Linsky, J. L., Weinstein, A., and Shine, R. A. 1977, *Ap. J.*, **214**, 785.
Hall, D. S. 1976, in *Multiple Periodic Variable Stars*, ed. W. S. Fitch (Dordrecht: Reidel), p. 287.
———. 1978, *A.J.*, **83**, 1469.
Heintz, W. D. 1975, *Ap. J.*, **195**, 411.
Herbig, G. H., and Spalding, J. F., Jr. 1955, *Ap. J.*, **121**, 118.
Hoffleit, D. 1964, *Catalogue of Bright Stars* (New Haven: Yale University Observatory).
Holm, A. 1979, Letter to IUE observers dated 1979 December 18.
Holt, S. S., White, N. E., Becker, R. H., Boldt, E. A., Mushotzky, R. F., Serlemitsos, P. J., and Smith, B. W. 1979, *Ap. J. (Letters)*, **234**, L65.
Iben, I., Jr. 1965, *Ap. J.*, **142**, 1447.
———. 1967, *Ann. Rev. Astr. Ap.*, **5**, 571.
Jamar, C., Macau-Hercot, D., Monfils, A., Thompson, G. I., Houziaux, L., and Wilson, R. 1976, *Ultraviolet Bright-Star Spectrophotometric Catalogue*, ESA Pub. SR-27.
Johnson, H. L. 1966, *Ann. Rev. Astr. Ap.*, **4**, 193.
Johnson, H. L., Mitchell, R. I., Iriarte, B., and Wisniewski, W. Z. 1966, *Comm. Lunar and Planet. Lab.*, **4**, 99.
Katsova, M. M., and Livshitz, M. A. 1978, *Soviet Astr.*, **22**, 208.
Kelch, W. L., Linsky, J. L., Basri, G. S., Chiu, H.-Y., Chang, S.-H., Maran, S. P., and Furenlid, I. 1978, *Ap. J.*, **220**, 962.
Kohl, J. L. 1977, *Ap. J.*, **211**, 958.
Kondo, Y., Morgan, T. H., and Modisette, J. L. 1976, *Ap. J.*, **207**, 167.
Kondo, Y., *et al.* 1979, *Ap. J.*, **230**, 526.
Kraft, R. P. 1967, *Ap. J.*, **150**, 551.
Labeyrie, A. 1975, *Ap. J. (Letters)*, **196**, L71.
Linsky, J. L. 1977, in *The Solar Output and Its Variation*, ed. O. R. White (Boulder: Colorado Associated University Press), p. 477.
Linsky, J. L., and Ayres, T. R. 1978, *Ap. J.*, **220**, 619.
Linsky, J. L., *et al.* 1978, *Nature*, **275**, 389.
Mewe, R., Heise, J., Gronenschild, E. H. B. M., Brinkman, A. C., Schrijver, J., and den Boggende, A. J. F. 1975, *Ap. J. (Letters)*, **202**, L67.
Noyes, R. W. 1974, contribution to IAU Colloquium No. 27, Cambridge, Mass.
Nugent, J., and Garmire, G. 1978, *Ap. J. (Letters)*, **226**, L83.
Parker, E. W. 1970, *Ann. Rev. Astr. Ap.*, **8**, 1.
Rottman, G. 1978, private communication.
Roussel-Dupre, R., Francis, M. H., and Billings, D. E. 1979, *M.N.R.A.S.*, **187**, 9.
Sandlin, G. D., Brueckner, G. E., and Tousey, R. 1977, *Ap. J.*, **214**, 898.
Shine, R. A., Lites, B. W., and Chipman, E. G. 1978, *Ap. J.*, **224**, 247.
Simon, T., Kelch, W. L., and Linsky, J. L. 1980, *Ap. J.*, in press.
Simon, T., and Linsky, J. L. 1980, preprint.
Simon, T., Linsky, J. L., and Schiffer, F. H., III. 1980, preprint.
Skumanich, A. 1972, *Ap. J.*, **171**, 565.

Smith, M. A. 1980, in *IAU Colloquium No. 51, Turbulence in Stellar Atmospheres*, ed. D. F. Gray and J. L. Linsky (New York: Springer), p. 126.
Smith, M. A., and Dominy, J. F. 1979, *Ap. J.*, **231**, 477.
Struve, O., and Kung, S. M. 1953, *Ap. J.*, **117**, 1.
Topka, K., Fabricant, D., Harnden, F. R., Jr., Gorenstein, P., and Rosner, R. 1979, *Ap. J.*, **229**, 661.
Tripp, D. A., Athay, R. G., and Peterson, V. L. 1978, *Ap. J.*, **220**, 314.
Uesugi, A., and Fukuda, I. 1970, Contribution Inst. Ap. and Kwasan Obs., University of Kyoto, No. 189.
Vaiana, G. S., and Rosner, R. 1978, *Ann. Rev. Astr. Ap.*, **16**, 393.
Vernazza, J. E., and Reeves, E. M. 1978, *Ap. J. Suppl.*, **37**, 485.
Vitz, R. C., Weiser, H., Moos, H. W., Weinstein, A., and Warden, E. S. 1976, *Ap. J. (Letters)*, **205**, L35.
Vogt, S. S., and Fekel, F. 1979, *Ap. J.*, in press.
Wallerstein, G. 1966, *Ap. J.*, **143**, 823.
Walter, F. M., Charles, P. A., and Bowyer, C. S. 1978, *A.J.*, **83**, 1539.
Walter, F. M., Linsky, J. L., Bowyer, S., and Garmire, G. 1980, *Ap. J. (Letters)*, in press.
White, O. R., and Lemaire, P. 1976, LASP *OSO 8* Rept. No. 2 (Boulder: University of Colorado).
Wilson, O. C. 1966, *Science*, **151**, 1487.
Wright, K. O. 1954, *Ap. J.*, **119**, 471.

T. R. Ayres: Laboratory for Atmospheric and Space Physics, University of Colorado, Boulder, CO 80309
J. L. Linsky: Joint Institute for Laboratory Astrophysics, University of Colorado, Boulder, CO 80309